# Ocean Alkalinity Enhancement - Avoiding runaway CaCO₃ precipitation during quick and hydrated lime dissolution

5    Charly A. Moras[1,*], Lennart T. Bach[2], Tyler Cyronak[3], Renaud Joannes-Boyau[1], Kai G. Schulz[1]

[1]Faculty of Science and Engineering, Southern Cross University, Lismore, NSW, Australia
[2]Institute for Marine and Antarctic Studies, Ecology & Biodiversity, University of Tasmania, Hobart, TAS, Australia
[3]Department of Marine and Environmental Sciences, Nova Southeastern University, Fort Lauderdale, FL, USA

*  *Correspondence to:* Charly A. Moras (c.moras.10@student.scu.edu.au)

**Abstract.** Ocean Alkalinity Enhancement (OAE) has been proposed as a method to remove carbon dioxide ($CO_2$) from the atmosphere and to counteract ocean acidification. It involves the dissolution of alkaline minerals such as quick lime, $CaO$, and hydrated lime, $Ca(OH)_2$. However, a critical knowledge gap exists regarding their dissolution in natural seawater. Particularly, how much can be dissolved before secondary precipitation of calcium carbonate ($CaCO_3$) occurs is yet to be established.

15   Secondary precipitation should be avoided as it reduces the atmospheric $CO_2$ uptake potential of OAE. Here we show that both $CaO$ and $Ca(OH)_2$ powders (>63 µm of diameter) dissolved in seawater within a few hours. However, $CaCO_3$ precipitation, in the form of aragonite, occurred at a saturation ($\Omega_{Ar}$) threshold of about 5. This limit is much lower than what would be expected for typical pseudo-homogeneous precipitation in the presence of colloids and organic materials. Secondary precipitation at unexpectedly low $\Omega_{Ar}$ was the result of so-called heterogeneous precipitation onto mineral phases, most likely onto $CaO$ and

20   $Ca(OH)_2$ prior to full dissolution. Most importantly, this led to runaway $CaCO_3$ precipitation by which significantly more alkalinity (TA) was removed than initially added, until $\Omega_{Ar}$ reached levels below 2. Such runaway precipitation would reduce the $CO_2$ uptake efficiency from about 0.8 moles of $CO_2$ per mole of TA down to only 0.1 mole of $CO_2$ per mole of TA. Runaway precipitation appears to be avoidable by dilution below the critical $\Omega_{Ar}$ threshold of 5, ideally within hours of the addition to minimise initial $CaCO_3$ precipitation. Finally, model considerations suggest that for the same $\Omega_{Ar}$ threshold, the

25   amount of TA that can be added to seawater would be more than three times higher at 5 °C than at 30 °C, and that equilibration to atmospheric $CO_2$ levels during mineral dissolution would further increase it by a factor of ~6 and ~3 respectively.

## 1 Introduction

Climate change is currently considered one of the largest threats to humankind (Hoegh-Guldberg et al., 2019; The Royal
Society and Royal Academy of Engineering, 2018; Ipcc, 2021). Global mean temperature have increased by 1.0 °C since pre-
industrial times, and could reach +1.2-1.9 °C in the next 20 years, and +2.1-5.7 °C by the end of this century (Ipcc, 2021).
Furthermore, up to 30% of anthropogenic $CO_2$ emissions have been taken up by the ocean through air-sea gas exchange,
leading to a decrease in the average open ocean pH of 0.1 units in a process termed ocean acidification – OA (Canadell et al.,
2007; Carter et al., 2019; Hoegh-Guldberg et al., 2007; Bates et al., 2012; Cyronak et al., 2014; Doney et al., 2009).
The $CO_2$ reduction pledges by the signatory states of the 2015 Paris Agreement aim to limit the negative impacts of global
warming and OA on ecosystems and human societies by limiting warming to less than +2.0 °C, ideally around +1.5 °C, by the
end of this century (Goodwin et al., 2018). However, current and pledged reductions will likely not be enough and additional
mitigation strategies are being discussed, such as o*cean alkalinity enhancement* – OAE (Gattuso et al., 2015; Lenton and
Vaughan, 2009; The Royal Society and Royal Academy of Engineering, 2018; Boyd et al., 2019). OAE is one with the highest
carbon dioxide removal potential, and modelling suggests that at a global scale, between 264 and 790 Gigatonnes (1 Gt = 1e12
kg) of atmospheric $CO_2$ could be removed by 2100 (Feng et al., 2017).
OAE typically relies on the dissolution of alkaline minerals in seawater, similar to what occurs during natural rock weathering
(Kheshgi, 1995). In this regard, magnesium-rich minerals such as brucite, periclase or forsterite, and calcium-rich minerals
such as quick and hydrated lime have been considered (Renforth and Henderson, 2017). The last two minerals are of particular
interest, due to their high solubility in seawater as well as their relatively rapid dissolution. Quick lime, also known as calcium
oxide (CaO), is obtained by the calcination of limestone, mainly composed of calcium carbonate ($CaCO_3$) and present in large
quantities in the Earth's crust (Kheshgi, 1995). Once heated to temperatures of ~1200 °C, each molecule of $CaCO_3$ breaks
down into one molecule of CaO and one molecule of $CO_2$ (Kheshgi, 1995; Ilyina et al., 2013). CaO can then be hydrated into
hydrated lime, also known as calcium hydroxide ($Ca(OH)_2$) (Kheshgi, 1995). The addition of either CaO or $Ca(OH)_2$ to
seawater leads to the dissociation of $Ca(OH)_2$ into one calcium $Ca^{2+}$ and two hydroxyl ions $OH^-$ (Feng et al., 2017; Harvey,
2008). Including the subsequent oceanic uptake of atmospheric $CO_2$, and ignoring the non-linearities of the seawater carbonate
system, i.e., changes in total alkalinity, TA, and dissolved inorganic carbon, DIC, are not 1:1, a conceptual model of CaO and
$Ca(OH)_2$ dissolution can be summarised as per:

$$(CaO + H_2O \rightleftharpoons Ca(OH)_2) + 2CO_2 \rightarrow Ca^{2+} + 2HCO_3^- \qquad\qquad 1$$
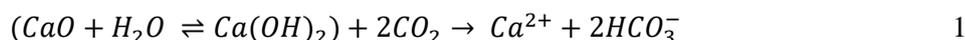
This chemical equation suggests that each mole of CaO or $Ca(OH)_2$ reacts with two moles of $CO_2$ to produce one mole of $Ca^{2+}$
and two moles of bicarbonate ions ($HCO_3^-$). A different way to look at this is that adding $Ca^{2+}$ to seawater increases TA by
two moles per mole of $Ca^{2+}$, while leaving the concentration of DIC unchanged (Wolf-Gladrow et al., 2007). This increases
the pH, lowering the $CO_2$ concentration, $[CO_2]$, and increasing the carbonate ion concentration, $[CO_3^{2-}]$ (Figure A 1, Appendix)

60 (Wolf-Gladrow et al., 2007; Dickson et al., 2007; Zeebe and Wolf-Gladrow, 2001). This in turn reduces the partial pressure of $CO_2$ ($pCO_2$) in seawater.

Depending on the amount of TA added and the initial seawater $pCO_2$, the water would either take up $CO_2$ from the atmosphere or degas less until equilibrium is restored, hence acting as a sink for atmospheric $CO_2$. Factoring in carbonate system non-linearities, about 1.6 moles of atmospheric $CO_2$ could be taken up per mole of CaO or $Ca(OH)_2$ (Köhler et al., 2010).

65 Furthermore, dissolving CaO and $Ca(OH)_2$ can also counteract OA in two ways, raising the pH of seawater and raising the calcium carbonate saturation state by increasing both dissolved $[Ca^{2+}]$ and $[CO_3^{2-}]$. Therefore, OAE is a dual solution for both removing $CO_2$ from the atmosphere and changing ocean acidification trajectories (Feng et al., 2017; Harvey, 2008; Boyd et al., 2019). However, major knowledge gaps exist regarding OAE, considering most research to date has been based on conceptual and numerical modelling (Feng et al., 2016; Renforth and Henderson, 2017; González and Ilyina, 2016; Mongin et

70 al., 2021). One of the major constraints is keeping $CaCO_3$ saturation state ($\Omega$) of the seawater below a critical threshold, beyond which $CaCO_3$ would precipitate inorganically. Such secondary precipitation would increase seawater $[CO_2]$ through decreasing $[CO_3^{2-}]$, and if all added alkalinity is being precipitated, only 1 mole of atmospheric $CO_2$ per mole of $Ca^{2+}$ would be removed, instead of about 1.6 without. If even more $CaCO_3$ precipitates, the efficiency would be further reduced.

The critical threshold for $\Omega$ with respect to the $CaCO_3$ mineral phase calcite, $\Omega_{Ca}$, has been determined experimentally for so-

75 called pseudo-homogeneous precipitation, i.e., in the presence of colloids and organic materials (Marion et al., 2009; Morse and He, 1993). For a salinity of 35 and at a temperature of 21 °C, the critical $\Omega_{Ca}$ value is ~18.8. Assuming a typical open-ocean TA and DIC concentrations, i.e., ~2350 µmol kg⁻¹ and ~2100 µmol kg⁻¹ respectively (Dickson et al., 2007), this threshold would be reached by an increase in TA of ~810 µmol kg⁻¹, corresponding to a critical threshold for $\Omega_{CaCO_3}$ with respect to aragonite, i.e., $\Omega_{Ar}$, of ~12.3. Furthermore, there are two other types of precipitation, i.e., homogeneous (in the absence of any

80 precipitation nuclei) and heterogeneous (in the presence of mineral phases), but these thresholds are poorly constrained (Marion et al., 2009).

A better understanding of dissolution and precipitation kinetics is needed to address knowledge gaps in OAE research. In order to do so, several dissolution experiments with CaO and $Ca(OH)_2$ were carried out to determine 1) how much alkaline material can be dissolved without inducing $CaCO_3$ precipitation, 2) what causes $CaCO_3$ precipitation, and 3) how it can be avoided if

85 observed.

## 2 Material & Methods

### 2.1 Experimental setup

Two different calcium minerals were sourced, calcium oxide (CaO) powder from Ajax Finechem (CAS no 1305-78-8) and an industrial calcium hydroxide ($Ca(OH)_2$) powder (Hydrated Lime 20kg, Dingo). The elemental composition of these powders

90 was analysed on Agilent 7700 Inductively Coupled Plasma Mass Spectrometer, coupled to a laser ablation unit NWR213 from

ESI. For that purpose, the samples were embedded in resin and calibrated against standard reference materials # 610 and #612 from the National Institute of Standards and Technology.

The dissolution experiments were conducted in natural seawater. The seawater was sampled about 200 to 300 m from the shore, avoiding collecting sand or silt, at Broken Head, New South Wales, Australia (28°42'12" S, 153°37'03" E). It was stored
95   up to 14 days at 4 °C in the dark to slow bacterial metabolic activity before being sterile-filtered using a peristaltic pump, connected to a 0.2 µm Whatman Polycap 75 AS filter. For salinity measurements, about 200 mL of seawater were placed in a gas-tight polycarbonate container and allowed to equilibrate to room temperature overnight. The sample's conductivity was then measured using a measuring cell (Metrohm 6.017.080), connected to a 914 pH/Conductometer. The conductivity was recorded in millisiemens per cm (mS/cm), and the temperature in °C. Salinity was calculated according to Lewis and Perkin
100   (1981) on the 1978 practical salinity scale.

## 2.2 OAE experiments

For each experiment, seawater was accurately weighed into high-quality borosilicate 3.3 2L or 5L Schott Duran beakers, and the temperature was controlled via a Tank Chiller Line TK 1000 set to 21 °C, feeding a re-circulation water jacket (Figure A 2, supplementary material). A magnetic stir bar was placed in the beaker, and the natural seawater was constantly stirred at
105   ~200rpm. To minimise gas exchange, a floating lid with various sampling ports was placed on top. Finally, after one hour of equilibration, calculated amounts of alkaline compounds were added. Upon addition, samples for DIC and TA were taken in increasing time intervals to fully capture the dissolution kinetics and check for potential secondary precipitation. Furthermore, the pH was monitored for the first hour before alkalinity addition, and over 5 hours after addition to determine when alkalinity was fully released. Once the maximum TA was reached, the entire content of the beaker was carefully transferred to a clean
110   Schott bottle of the corresponding volume. The bottles were kept in the dark for the duration of each experiment, i.e., up to 48 days, with the same constant stirring of ~200 rpm at 21 °C. Each bottle was exposed to UV light for at least 30 minutes after each sampling to avoid bacterial growth.

### 2.2.1 CaO and Ca(OH)$_2$ dissolution

The additions of sieved CaO and Ca(OH)$_2$ were performed using a 63 µm mesh. The mesh was placed in a clean upside-down
115   50 mL Falcon tube cap, avoiding losing any material smaller than 63 µm when weighing, and the overall weight was recorded. Then, the mesh was placed above the Schott bottle, and mineral was added by gently tapping the side of the sieve. Finally, the sieve was placed in the same upside-down Falcon tube cap and the weight of the whole setup was recorded again, making sure that the desired amount had been added. The weighing steps were carefully performed to avoid material loss between the bottle and the balance, and was achieved in less than 5min. Two alkalinity additions, +250 and +500 µmol kg$^{-1}$ with each calcium
120   powder were performed (Table 1).

### 2.2.2 Na₂CO₃ alkalinity and particles addition and filtration

A 1M solution of sodium carbonate ($Na_2CO_3$, CAS number 497-19-8) was freshly prepared before the experiment. Ultrapure $Na_2CO_3$ (CAS number 497-19-8) was accurately weighed into a clean 100 mL Schott bottle and made up to 100g with MilliQ (18.2 MΩ). The solution was then sonicated for 15 minutes with gentle shaking. The amount of $Na_2CO_3$ to be added was

125    calculated so that a similar maximum $\Omega_{Ar}$ would be reached, i.e., ~7.7, as in the previous experiments with the highest addition of CaO and $Ca(OH)_2$. This required almost twice the alkalinity increase as before (Table 1), because $Na_2CO_3$ additions concomitantly increase DIC when dissociating in two sodium ions, i.e., $Na^+$, and one $CO_3^{2-}$, making the $\Omega_{CaCO3}$ increase smaller. Calculations were done in CO₂SYS (see below).

In another, otherwise identical, experiment with the $Na_2CO_3$ solution, quartz powder was added after two days. The addition

130    of quartz powder was similar to the sieved CaO and $Ca(OH)_2$ addition, i.e., through a 63 µm mesh. The amount of quartz particles added was determined to provide the same amount of mineral surface as for the $Ca(OH)_2$ experiments with a TA increase of 500 µmol kg⁻¹. It was calculated using densities and masses for $Ca(OH)_2$ and quartz, and assuming spherical particles with a diameter of 63 µm. Quartz powder was chosen as it does not dissolve on timescales relevant to the experiment and hence does not supply extra TA (Montserrat et al., 2017).

135    Finally, a particle filtering experiment was carried out using $Ca(OH)_2$ as the alkaline compound following the same setup as described above. Here we first added $Ca(OH)_2$ to increase TA by ~500 µmol kg⁻¹ (Table 1). After 4h of reaction, the entire content of the 2L Schott beaker was filtered through a nylon Captiva Econofilter (25mm) with a pore size of 0.45 µm into a clean 1L Schott bottle using a peristaltic pump. The bottle was filled from bottom to top, with overflow to minimise gas exchange.

140    **2.2.3 Dilution experiments**

A last set of experiments diluted alkalinity enriched samples with natural seawater over time, to test if secondary precipitation can be avoided through dilution. $Ca(OH)_2$ was added to reach a final alkalinity enrichment of 500 and 2000 µmol kg⁻¹. These initial concentrations were then diluted with NSW in several steps as described in the following.

For the experiment with a targeted TA increase of 500 µmol kg⁻¹, two 5L Schott bottles were filled with 5kg of natural seawater

145    and placed on a magnetic stirring platform. Calculated amounts of $Ca(OH)_2$ were added to the first bottle, while the natural seawater in the second bottle was left for future dilutions. Both bottles were kept on the same bench under the same conditions, both stirring at a rate of ~200rpm, for the duration of the experiment. $Ca(OH)_2$ powder was added as described above using the 63 µm sieve. Following the $Ca(OH)_2$ addition, 1:1 dilutions were performed in 1L Schott bottles that were kept in the dark and placed on a magnetic platform at a stirring rate of ~200rpm. After each sampling, the bottles were exposed to UV light for

150    at least 30 minutes. The second dilution experiment was set up like the first one, the only difference being that the targeted TA increase was 2000 µmol kg⁻¹. The dilution ratio was 1:7 to, again, reduce the targeted TA increase to 250 µmol kg⁻¹. All dilutions were performed 10 minutes, 1 hour, 1 day and 1 week after $Ca(OH)_2$ addition.

### 2.3 Carbonate chemistry measurements

Samples for TA and DIC were filtered through a nylon Captiva Econofilter (0.45 µm) using a peristaltic pump into 100 mL
155    Borosilicate 3.3 Schott DURAN glass stopper bottles. The bottles were gently filled from the bottom to top, using a 14-gauge
needle as described in Schulz et al. (2017), with at least half of their volume overflow (Dickson et al., 2007). 50µL of saturated
mercuric chloride solution was added to each sample before being stored without headspace in the dark at 4 °C. TA was
analysed via potentiometric titrations on an 848 Titrino Plus coupled to an 869 Compact Sample Changer from Metrohm using
0.05M HCl, with the ionic strength adjusted to 0.72 mol kg$^{-1}$, corresponding to a salinity of 35 with NaCl. Titrations and
160    calculations followed the open-cell protocols by Dickson et al. (2007). DIC was measured using an Automated Infra-Red
Inorganic Carbon Analyzer (AIRICA) coupled to a LICOR Li7000 Infra-Red detector as described in Gafar and Schulz (2018).
Measured values of TA and DIC were corrected using an internal Standard prepared as per Dickson et al. (2007) which had
been calibrated against Certified Reference Materials Batch #175 and #190 (Dickson, 2010).

### 2.4 Particulate Inorganic Carbon and Scanning Electron Microscopy (SEM)

165    Samples for total particulate carbon (TPC) and particulate organic carbon (POC) were collected at the end of some experiments
on pre-combusted (450 °C) GF/F filters, and stored frozen until analysis. Then, POC filters were fumed with HCl for 2 hours
before drying over night at 60 °C while TPC filters were dried untreated. Both TPC and POC were quantified on an Elemental
Analyser Flash EA, Thermo Fisher, coupled to an Isotope Ratio Mass Spectrometer (IRMS), Delta V Plus. Particulate
inorganic carbon (PIC), or $CaCO_3$, was calculated from the difference between TPC and POC. The results are reported in µmol
170    kg$^{-1}$ with an uncertainty estimate calculated by an error propagation from the square root of the sum of the squared standard
deviations for TPC and POC. Finally, samples of CaO and $Ca(OH)_2$ were analysed for their carbon content. This analysis
aimed to identify the presence and estimate the amount of particulate carbon, most likely $CaCO_3$, in the respective mineral
powders.

When $CaCO_3$ was suspected to have precipitated in the experiments, samples for SEM analysis were taken. For that purpose,
175    10 to 15 mL of the sample water was collected on polycarbonate Whatman Cyclopore filters with a 0.2 µm pore size, and
rinsed with 50 mL of MilliQ. The filters were dried at 60 °C overnight and kept in a desiccator until analysis on a tabletop
Scanning Electron Microscope TM4000 Plus from Hitachi, coupled to an Energy Dispersive X-Ray (EDX) Analyser, allowing
to identify the morphotype and elemental composition of precipitates.

### 2.5 Carbonate chemistry calculations

180    Most seawater parameters were calculated using the $CO_2SYS$ script for MATLAB® (MathWorks), using the dissociation
constants for carbonic acid by Lueker et al. (2000) and for boric acid by Uppstrom (1974). With two measured carbonate
chemistry parameters, i.e., DIC and TA, most of the others can be calculated straight away. An exception in our experiments

was that the addition of CaO and Ca(OH)$_2$ changes the calcium concentration and hence the salinity-based $\Omega_{CaCO3}$ calculated by CO$_2$SYS is erroneous. $\Omega_{CaCO3}$ is defined by the solubility product of CaCO$_3$ as:

185

$$\Omega_{CaCO3} = \frac{[Ca^{2+}] \times [CO_3^{2-}]}{K_{sp}} \qquad 2$$

where [Ca$^{2+}$] and [CO$_3^{2-}$] denote seawater concentration of Ca$^{2+}$ and CO$_3^{2-}$, and K$_{sp}$ the solubility product for calcite or aragonite. To calculate saturation states, CO$_2$SYS was used to determine K$_{sp}$ and [CO$_3^{2-}$] from measured DIC and TA. The correct calcium concentration [Ca$^{2+}$]$_{Corr}$ was estimated from measured salinity (Riley and Tongudai, 1967) plus half the amount

190    of alkalinity that was generated during CaO or Ca(OH)$_2$ dissolution or lost due to CaCO$_3$ precipitation $\Delta$TA:

$$[Ca^{2+}]_{Corr} = \frac{0.02128}{40.087} \times \frac{Salinity}{1.80655} + \frac{\Delta TA}{2} \qquad 3$$

The corrected $\Omega_{Ca}$ and $\Omega_{Ar}$ were then calculated from in-situ [CO$_3^{2-}$], [Ca$^{2+}$]$_{Corr}$ and K$_{sp}$. Please note that we have opted to rather report $\Omega_{Ar}$ than $\Omega_{Ca}$ since aragonite is more likely to be precipitated in natural seawater (Berner, 1975; Riebesell et al.,

195    2011; Zeebe and Wolf-Gladrow, 2001).

### 3 Results

#### 3.1 Chemical composition of CaO and Ca(OH)$_2$

The chemical composition of the CaO and Ca(OH)$_2$ powders were analysed for their major ions. As to be expected, both consisted mainly of calcium, with minor contributions by magnesium and silicon (see Table A 1, Appendix, for a more

200    extensive list). Furthermore, CaO and Ca(OH)$_2$ contained about 9.4 ±0.1 mg g$^{-1}$ and 18.0 ±0.2 mg g$^{-1}$ of particulate carbon respectively, i.e., ~0.9% and ~1.8%.

#### 3.2 CaO dissolution in filtered natural seawater

In the first CaO experiment with ~250 µmol kg$^{-1}$ TA addition, TA increased by ~200 µmol kg$^{-1}$ within the first 4 hours (Figure 1a). Following this increase, TA was stable over time. In contrast, DIC increased slowly over time, reaching about +50 µmol

205    kg$^{-1}$ on day 47 of the experiment (Figure 1b). Finally, $\Omega_{Ar}$ showed a similar trend to the $\Delta$TA, increasing from ~2.9 to ~5.1 within the first 4 hours before slowly decreasing to 5.0 as of day 47 (Figure 1c).

In the second CaO experiment with about 500 µmol kg$^{-1}$ TA addition, TA increased by ~410 µmol kg$^{-1}$ within the first 4 hours before slowly decreasing two days later (Figure 1a), followed by more rapid decreases over the following week, before slowing down and eventually reaching steady state at a $\Delta$TA of about -540 µmol kg$^{-1}$. This corresponds to a total loss of TA of ~950

210   μmol kg$^{-1}$. Similarly, a slight decrease in DIC of ~10 μmol kg$^{-1}$ was observed over the first two days before a much more considerable reduction in the following week before levelling off at a ΔDIC of about ~465 μmol kg$^{-1}$ (Figure 1b). Finally, $\Omega_{Ar}$ increased rapidly during the first 4 hours of the experiment from 2.8 up to 7.6 (Figure 1c). Following this quick increase, $\Omega_{Ar}$ decreased by 0.3 units within the first two days before rapidly dropping to 2.4 on day 13, and reaching ~1.8 on day 47, corresponding to a reduction of 1.0 compared to the starting value.

### 215   3.3 Ca(OH)$_2$ dissolution in filtered natural seawater

In the first Ca(OH)$_2$ experiment with a TA addition of ~250 μmol kg$^{-1}$, TA increased by ~220 μmol kg$^{-1}$ after 4h of reaction, before stabilising at a ΔTA of ~210 μmol kg$^{-1}$ for the rest of the experiment (Figure 2a). The DIC concentration increased steadily following the TA addition by ~70 μmol kg$^{-1}$ until the end of the experiment (Figure 2b). Finally, $\Omega_{Ar}$ reached ~4.1 after 4 hours, slightly decreasing over time, down to 3.3 on day 28 (Figure 2c).

220   In the second Ca(OH)$_2$ experiment with a TA addition of ~500 μmol kg$^{-1}$, TA increased by ~440 μmol kg$^{-1}$ within the first 4h (Figure 2a). This was followed by a relatively steady decrease over the next 2 weeks, after which the decrease accelerated before levelling off at a ΔTA of about -420 μmol kg$^{-1}$ towards the end of the experiment. Overall, ~860 μmol kg$^{-1}$ of TA was lost compared to the highest TA recorded. The DIC concentration decreased as well, dropping in a similar fashion as TA and reaching a ΔDIC of about -395 μmol kg$^{-1}$ compared to the initial DIC concentration (Figure 2b). Finally, $\Omega_{Ar}$ increased from 225   2.5 to 7.4 in the first 4 hours before decreasing, similarly to TA and DIC, reaching ~2.0 on day 42 (Figure 2c).

### 3.4 Na$_2$CO$_3$, particle filtration and addition

Three experiments assessed the influence of particles on CaCO$_3$ precipitation. In the first one, ~1050 μmol kg$^{-1}$ of TA was added using a 1M Na$_2$CO$_3$ solution, designed to result in a similar maximum $\Omega_{Ar}$ as in the previous experiments when TA precipitated (Table 1). Upon addition, TA increased by ~1060 μmol kg$^-$ and DIC by ~530 μmol kg$^{-1}$ within minutes. For the 230   remainder of the experiment, ΔTA was fairly constant between 1060 and 1040 μmol kg-1 (Figure 3a). In contrast, DIC slightly increased over 42 days from a ΔDIC of ~530 μmol kg$^{-1}$ on day 1 to ~560 μmol kg$^{-1}$ on day 42 (Figure 3b). Finally, $\Omega_{Ar}$ increased from ~2.3 to ~8.5 within minutes and slightly decreased to ~8.1 after 42 days of experiment (Figure 3c).

In the second experiment, the addition of aliquots of 1M Na$_2$CO$_3$ solution (Table 1) increased TA by 1070 μmol kg$^{-1}$, while DIC increased by ~540 μmol kg$^{-1}$ within minutes and remained stable (Figure 3a, 3b). Then, after 2 days, quartz was added. 235   While one day later ΔTA and ΔDIC remained unchanged, about a week later, ΔTA had decreased to ~220 μmol kg$^{-1}$ while ΔDIC had dropped to ~120 μmol kg$^{-1}$ (Figure 3a, 3b). Over the next month, ΔTA and ΔDIC kept on decreasing, although at a slowing pace, reaching about -200 and -110 μmol kg$^{-1}$ respectively. Finally, $\Omega_{Ar}$ followed a similar trend, with an increase from ~2.8 up to ~9.2 within the first 1.5 hours, and a pronounced decline to ~2.0 at the end of the experiment.

In the last experiment, Ca(OH)$_2$ was added for a TA increase of 500 μmol kg$^{-1}$ (Table 1), a level at which a significant TA 240   decrease had been observed after 5 hours previously (Figure 2a). In contrast, however, upon filtration of the entire experimental bottle content after reaching ~470 μmol kg$^{-1}$ at the 4-hour mark, ΔTA remained relatively constant between 465 and 470 μmol

kg-1 over the following 48 days of experiment (Figure 3a). ΔDIC increased from ~5 to 55 µmol kg$^{-1}$ after filtration (Figure 3b). Finally, $\Omega_{Ar}$ increased from ~2.8 to ~8.2 within the first 1.5 hours, and then slightly decreased to ~7.5 over the 48 days of experiment (Figure 3c).

### 3.5 Dilution experiments

#### 3.5.1 500 µmol kg$^{-1}$ addition

In this set of experiments with a TA addition of ~500 µmol kg$^{-1}$ by Ca(OH)$_2$, ΔTA increased similarly to the other Ca(OH)$_2$ experiment to ~450 µmol kg$^{-1}$ after 2 hours. These changes in TA were followed by a decline to ~320 µmol kg-1 after 14 days, although the latter being a slightly slower decrease than previously (Figure 4a, 4d). After a first increase in ΔDIC by ~10 µmol kg$^{-1}$ on day 1, it steadily decreased to about -20 µmol kg$^{-1}$ after two weeks (Figure 4b, 4e). Finally, $\Omega_{Ar}$ was calculated, to increase from ~2.7 to ~7.8 after 2 hours, before steadily decreasing to ~6.4 on day 14 (Figure 4c, 4f).

After 10 minutes, 1 hour, 1 day, and 1 week, dilutions of the ~500 µmol kg$^{-1}$ of TA by Ca(OH)$_2$ addition were performed. In these diluted samples, ΔTA remained relatively stable over time, until the end of the experiments on day 29, regardless of dilution time (Figure 4a, 4d). Upon dilution, ΔTA was reduced, being very similar for the 10 minutes, 1 hour and 1 day dilutions. Overall, ΔTA in the 1 week dilution, however, was slightly lower. In all dilutions, ΔDIC increased over time, ranging between ~20 µmol kg$^{-1}$ and ~60 µmol kg$^{-1}$, independent of dilution timing. Finally, $\Omega_{Ar}$ showed similar trends like ΔTA, reaching between ~4.8 and ~5.2, slightly decreasing over time until end of the experiment.

#### 3.5.2 2000 µmol kg$^{-1}$ addition

Similarly to the previous experiment, this experiment consisted of a TA increase of ~2000 µmol kg$^{-1}$ by Ca(OH)$_2$ addition. The TA only increased to ~⅓ of the theoretical alkalinity addition, i.e., ~725 µmol kg$^{-1}$ within the first two hours (Figure 4a, 4d). Following this increase, TA rapidly decreased during the first day, reaching a ΔTA of about -1260 µmol kg$^{-1}$, and -1440 µmol kg$^{-1}$ in the following week (Figure 4a, 4d). From then on, TA appeared to stabilise up to day 14, before slightly increasing until day 21. A similar trend was observed for ΔDIC, decreasing by ~580 µmol kg$^{-1}$ within the first two hours, before radically dropping to about -1590 µmol kg$^{-1}$ on day 1, and -1660 µmol kg$^{-1}$ after 7 days (Figure 4b, 4e). Over the remaining 41 days, ΔDIC then increased by ~210 µmol kg$^{-1}$, although remaining about 1450 µmol kg$^{-1}$ under the starting DIC concentration. Finally, $\Omega_{Ar}$ reached up to ~16.7 after 2 hours of reaction, followed by a rapid drop down to ~3.2 on day 1 and ~2.0 on day 14, while slightly increasing the following 34 days, varying between 2.0 and 2.1 (Figure 4c, 4f).

Dilutions were performed after 10 minutes, 1 hour, 1 day and 1 week after Ca(OH)$_2$ addition, in this case in a 1:7 ratio. Concerning ΔTA, ΔDIC and $\Omega_{Ar}$, the 10 minutes and 1 hour dilutions showed similar responses, as did the 1 day and 1 week dilutions. Upon dilution, ΔTA reached values ~240 µmol kg$^{-1}$ after the 10 minutes and 1 hour dilutions, and about -160 to -190 µmol kg$^{-1}$ for the 1 day and 1 week dilutions. With the exception of one data point in the 1 week dilution time data, ΔTA remained relatively constant throughout all dilution experiments (Figure 4a, 4d). DIC changes were similar to the TA changes,

with very similar values reached for the 10 minutes and 1 hour dilutions, as opposed to the 1 day and 1 week ones (Figure 4b, 4e). In all dilutions, $\Delta$DIC slowly increased over time. Finally, $\Omega_{Ar}$ dropped to ~5.0-5. in the 10 minutes and 1 hour dilutions, while it dropped to ~2.3-2.8 (1:7) in the 1 day and 1 week dilution. In all experiments, $\Omega_{Ar}$ decreased slightly over time after dilutions (Figure 4c, 4f).

### 3.6 Particulate inorganic carbon

With the exception of the ~1050 TA addition by $Na_2CO_3$ plus quartz particles, measured PIC in experiments was always higher than estimates from measured $\Delta$TA (Table 2). Furthermore, PIC estimated from the theoretically maximum TA increase upon full mineral dissolution, $\Delta TA_{Theo}$, was always higher than estimated PIC from $\Delta$TA, by about 30% in the ~500 µmol kg⁻¹ TA additions, and almost 90% in the ~2000 µmol kg⁻¹ TA addition.

### 4 Discussion

This study presents the first results on the dissolution of CaO and $Ca(OH)_2$ in natural seawater in the context of ocean alkalinity enhancement. In some of our experiments, secondary precipitation was detected. More specifically, we observed "runaway $CaCO_3$ precipitation" at TA additions equal or higher than 500 µmol kg⁻¹, i.e., not only was the added TA completely removed, but significant portions of residual seawater TA as well, until a new steady state was reached. This would vastly reduce the desired $CO_2$ removal potential by OAE and should therefore be avoided. Hence, in a set of experiments, we simulated ocean mixing to test required timescales to avoid secondary $CaCO_3$ precipitation for applications that initially had TA additions above the critical threshold.

### 4.1 Identifying $CaCO_3$ precipitation and the problem of not measured precipitation

$CaCO_3$ precipitation can occur via three pathways, i.e., heterogeneous, homogeneous and pseudo-homogeneous nucleation and precipitation (Marion et al., 2009; Chen et al., 2005; Wolf et al., 2008). Heterogeneous precipitation relies on the presence of existing solid mineral phases. This differs from homogeneous precipitation, characterised by the formation of $CaCO_3$ crystals from $Ca^{2+}$ and $CO_3^{2-}$ ions present in the solution in the absence of any nucleation surfaces (Chen et al., 2005; Wolf et al., 2008). Finally, the last type of precipitation, termed pseudo-homogeneous, is similar to homogeneous nucleation, however it occurs on nuclei other than solid minerals such as colloids, organic particles or glassware in a laboratory setting (Marion et al., 2009). Concerning the $\Omega_{CaCO_3}$ thresholds beyond which $CaCO_3$ precipitation is expected to occur, the lowest would be for heterogeneous and the highest for homogeneous, with pseudo-homogeneous nucleation in between.

When 1 mole of $CaCO_3$ is precipitated, the TA of the solution decreases by 2 moles because of the removal of $CO_3^{2-}$ ions, accounting for 2 moles of TA (Equation 1). Simultaneously, the loss of 1 mole of $CO_3^{2-}$ ions decrease the DIC concentration by 1 mole. Hence, any loss of TA and DIC following a 2:1 ratio can be linked to $CaCO_3$ precipitation. When $CaCO_3$ precipitation was suspected in our experiments, SEM and particulate inorganic carbon samples were taken to confirm the

presence of $CaCO_3$ and to identify which morphotypes were predominant. In the $+250\ \mu mol\ kg^{-1}$ TA additions by CaO and $Ca(OH)_2$, both appeared to fully dissolve without inducing $CaCO_3$ precipitation, as TA and $\Omega_{Ar}$ quickly increased within

minutes until reaching their respective maximum after about a day and remaining stable over weeks (Figure 1a and 1c, Figure 2a and 2c) A slight increase in DIC was observed over time, expected when atmospheric $CO_2$ is ingassing from the headspace. This in turn lead to slowly decreasing $\Omega_{CaCO3}$ at constant TA, when increasing DIC and $[CO_2]$, lowering the pH and $[CO_3^{2-}]$ (Equation 2). The reason why the measured TA increase was slightly below the theoretically expected one is most likely a combination of impurities present (in the case of CaO, a significant fraction could be hydrated), and loss of the finely ground

material during the weighing and sieving process despite all efforts. On average, ~25-27% of alkalinity added was not measured in the experiments with CaO, and about 13-17% in the experiments with $Ca(OH)_2$ (Table 1, Figure 1 and Figure 2) In contrast, in the $+500\ \mu mol\ kg^{-1}$ TA additions by CaO and $Ca(OH)_2$ additions, TA started decreasing after about 4 hours, upon the initial increase. This decrease in TA was accompanied by a decrease in DIC. In the CaO experiment (exactly the same conclusions could be reached for the $Ca(OH)_2$ experiment), TA reached a maximum of about $+410\ \mu mol\ kg^{-1}$ after 4

hours of reaction, before dropping to about $-560\ \mu mol\ kg^{-1}$ after 34 days, constituting an overall loss of about $-970\ \mu mol\ kg^{-1}$. If this TA loss would be by $CaCO_3$ precipitation, DIC should be reduced by half this amount, i.e., about $-485\ \mu mol\ kg^{-1}$. And indeed, measured DIC loss was exactly the same, suggesting that TA was precipitated in the form of $CaCO_3$. Although a perfect match, a caveat here is that the DIC loss is underestimated as of concurrent ingassing of $CO_2$ from the head space, becoming visible when precipitation ceases towards the end (Figure 1b). Hence, the DIC loss should have been higher,

requiring also higher TA removal than actually measured. This discrepancy can be explained by the fact that the maximum increase in TA from full dissolution of CaO or $Ca(OH)_2$ cannot be measured in the presence of concurrent $CaCO_3$ precipitation. This is mostly evident in the $+2000\ \mu mol\ kg^{-1}$ TA addition (Figure 4), where DIC decreases due to $CaCO_3$ precipitation, yet TA increases due to higher $Ca(OH)_2$ dissolution rates. It also explains why estimated PIC calculated from measured TA changes are smaller than actually measured PIC concentrations (Table 2). In the experiment with 1M $Na_2CO_3$ and quartz

particles, both estimated PIC have similar results. However, the measured PIC is about twice as low. This could be explained by a combination of precipitation on both the quartz particles and bottle walls. In this sense, trying to estimate $CaCO_3$ precipitation from measured changes in TA, without considering theoretical TA generation by dissolution or actual PIC measurements, might underestimate total precipitation. Finally, next to impurities and issues with mineral handling, the reason why measured seawater PIC concentrations are in between the other estimates lies in the fact that a small portion of the $CaCO_3$

precipitated on the bottle walls, at least in the $2000\ \mu mol\ kg^{-1}$ TA experiment. While being a laboratory artefact, this has no practical consequences as in a natural setting, the TA would eventually precipitate in the water column.

## 4.2 The presence of mineral phases enhances $CaCO_3$ precipitation

An interesting finding in our experiments was that whenever $CaCO_3$ precipitation was observed, it continued even if the solution dropped below an $\Omega_{Ar}$ of ~4-5, levels at which no precipitation was observed in the $+250\ \mu mol\ kg^{-1}$ TA addition experiments. Furthermore, in all these experiments, precipitation decreased and seemingly ceased at a $\Omega_{Ar}$ of ~1.8-2.0. It

appears that when $CaCO_3$ is initially precipitated, $CaCO_3$ continues to precipitate in a runaway fashion, even if $\Omega_{Ar}$ drops below levels where precipitation would not be initiated in natural seawater. This is to be expected as precipitation rates of $CaCO_3$ into $CaCO_3$ mineral phases are directly related to $\Omega_{CaCO3}$, decreasing exponentially until reaching zero at an $\Omega_{CaCO3}$ value of 1 (Zhong and Mucci, 1989; Morse et al., 2007). However, why did precipitation occur at a much lower $\Omega_{CaCO3}$, i.e.

340    $\Omega_{Ar}$ ~7.5, than expected, i.e., ~12.3 (Marion et al., 2009)? It is known that the presence of particles in suspension can initiate and accelerate $CaCO_3$ precipitation (Millero et al., 2001; Morse et al., 2003; Wurgaft et al., 2021). It is unlikely that the presence of $CaCO_3$ impurities in CaO (less than 1% carbon) and $Ca(OH)_2$ (less than 2% carbon) from imperfect calcination would have caused precipitation, as the presence of $CaCO_3$ mineral phases should have caused precipitation at any saturation state above 1, i.e., also in the +250 µmol kg$^{-1}$ TA addition experiments. Furthermore, modelling precipitation using

345    experimentally determined $\Omega_{Ar}$ and surface area dependant aragonite precipitation rates onto $CaCO_3$ mineral phases suggests that once precipitation becomes analytically detectable, it should proceed very rapidly before levelling off, i.e., within a couple of days (Zhong and Mucci, 1989). However, that is in contrast to what we observed here. We observed the bulk of precipitation occurring over a period of at least a week, with apparent differences between the different dissolving minerals (i.e., CaO, $Ca(OH)_2$ and quartz, although it is acknowledged that experiments were not replicated).

350    Another explanation is heterogeneous precipitation on not yet dissolved CaO and $Ca(OH)_2$ particles (or other impurities), leading to $CaCO_3$ crystal formation and initiating runaway precipitation. The $\Omega_{Ar}$ threshold for this process would depend on lattice compatibility of the mineral phases (Tang et al., 2020). For instance, $CaCO_3$ precipitation has been observed at any saturation states above 1 when introducing $CaCO_3$ seed particles. In contrast, the addition of quartz particles did not trigger precipitation at an $\Omega_{Ar}$ of up to 3.5 (Lioliou et al., 2007). For that to occur, $\Omega_{Ar}$ would need to be further increased. And indeed,

355    above an $\Omega_{Ar}$ of ~9.2, $CaCO_3$ precipitation did actually occur (Figure 3). The reason for an initially slower but then more rapid precipitation could be a combination of exponentially increasing $CaCO_3$ surface area, as well as concomitantly increasing lattice compatibility (Lioliou et al., 2007; Pan et al., 2021). The filtration of TA enriched seawater supports this idea. Not yet dissolved mineral phases that could facilitate early nucleation are removed, preventing runaway $CaCO_3$ precipitation (Figure 3).

360    Needle-shaped aragonite precipitation onto quartz particles (Figure 5c and 5d) was directly observed by SEM imaging, and confirmed by EDX analysis, identifying the larger base mineral to be rich in silicon, a key characteristic of quartz, and the needle-shaped particles composed of carbon, oxygen and calcium (Chang et al., 2017; Ni and Ratner, 2008; Pan et al., 2021). In contrast, aragonite precipitation in the +500 µmol kg$^{-1}$ TA addition by CaO and $Ca(OH)_2$ did not reveal any insoluble base-element other than Ca, suggesting initial $CaCO_3$ precipitation onto CaO and $Ca(OH)_2$ (Figure 5a and 5b). In some situations

365    (Figure 5b), round crystals were also observed, suggesting the presence of vaterite (Chang et al., 2017). However, aragonite crystals represented the majority of $CaCO_3$ observed by SEM. Early $CaCO_3$ precipitation onto CaO and $Ca(OH)_2$ particles, providing some sort of coating could also, or at least partially, explain why maximum measured TA was lower than theoretically anticipated.

### 4.3 Impacts of CaCO₃ precipitation on OAE potential

370 From an OAE perspective, $CaCO_3$ precipitation is an important chemical reaction that needs to be avoided. When $CaCO_3$ precipitates, TA and DIC decrease in a 2:1 fashion. Simultaneously, dissolved $[CO_3^{2-}]$ and $\Omega_{CaCO_3}$ are decreasing, and $[CO_2]$ is increasing, impacting OAE potential. Considering typical open ocean TA and DIC concentrations of 2350 and 2100 µmol kg$^{-1}$ respectively, at a salinity of 35 and a temperature of 19 °C, this water mass would have a pCO₂ close to atmospheric equilibrium, ~416 ppm, a pH$_T$ value (total scale) of ~8.04, and an $\Omega_{Ar}$ of ~2.80. Without $CaCO_3$ precipitation, an addition of

375 500 µmol kg$^{-1}$ TA would lower pCO₂ to ~92 µatm and increase pH$_T$ and $\Omega_{Ar}$ to about 8.61 and 8.45 respectively. If fully equilibrated with the atmosphere, DIC would increase by about 420 µmol kg$^{-1}$, leading to a pH$_T$ and $\Omega_{Ar}$ 0.07 and 1.10 higher than prior to the addition, respectively (Table 3). The resulting OAE efficiency would be 0.83 mole of atmospheric CO₂ absorbed per mole of TA, very similar to estimates by Köhler et al. (2010). Considering that $CaCO_3$ is the base material for CaO and Ca(OH)₂, and the fact that 2 moles of TA are produced per mole of mineral dissolution, ~0.7 tonnes of CO₂ could be

380 captured per tonne of source material, assuming CO₂ capture during the calcination process. At a global-scale, using all available ship capacity and assuming a slow discharge of 1.7 to 4.0 Gt of Ca(OH)₂ per year, between 1.2 and 2.8 Gt of CO₂ per year could be absorbed by the ocean (Caserini et al., 2021). Similarly, following the models from Feng et al. (2016) with a constant addition of Ca(OH)₂ at 10 Gt.year$^{-1}$, we could expect to absorb about 7 Gt of CO₂ per year. This would eventually lead to more than 546 Gt of CO₂ by 2100 if implemented in 2022.

385 However, these substantial numbers assume a complete dissolution without $CaCO_3$ precipitation. If as much $CaCO_3$ precipitates as TA was added, only 0.50 mole of DIC can be absorbed per mole of TA after equilibration with atmospheric pCO₂ (Table 3). This represent a decrease by nearly 40% in OAE potential. Similarly, assuming runaway $CaCO_3$ precipitation until $\Omega_{Ar}$ = 2.0 decreases the OAE potential further by almost 90%. Then, only ~0.11 mole of DIC would be absorbed per mole of TA added (Table 3). Finally, secondary $CaCO_3$ precipitation higher than TA addition will lead to pH$_T$ and $\Omega_{CaCO_3}$ levels

390 lower than initial ones. For instance, runaway precipitation for a TA addition of 500 µmol kg$^{-1}$ will see pH$_T$ drop by about 0.1 from 8.04 to 7.93 and $\Omega_{Ar}$ from 2.80 to 1.66, significantly enhancing ongoing ocean acidification (Table 3). Runaway $CaCO_3$ precipitation for a TA addition of 1000 µmol kg$^{-1}$ would even see $\Omega_{Ar}$ drop below 1. Under such conditions, aragonite, an important biomineral for a variety of marine organisms, e.g., sessile corals, benthic molluscs and planktonic pteropods, would start to dissolve (Zeebe and Wolf-Gladrow, 2001; Riebesell et al., 2011). In summary, runaway $CaCO_3$ precipitation in OAE

395 has to be avoided as not only reducing CO₂ uptake efficiency significantly but also enhancing ocean acidification. Keeping track of OAE efficiency from changes in TA concentrations can be challenging as $CaCO_3$ precipitation can be underestimated as described earlier, requiring new and clever monitoring strategies to ensure effective dilutions take place.

### 4.4 Avoiding CaCO₃ precipitation by dilution and other TA addition strategies

While above considerations stress the importance for monitoring $CaCO_3$ precipitation, they do not take into account the natural

400 dilution that would occur in the wake of ships releasing TA in the ocean, or by natural mixing of TA-enriched water with

surrounding seawater (Caserini et al., 2021; Feng et al., 2017; Mongin et al., 2021). In our experiments, a 1:1 dilution of seawater in which $CaCO_3$ precipitation was taking place upon a 500 µmol kg$^{-1}$ TA addition was seemingly stopped, even if initiated only after one week. This comes a bit at a surprise as precipitation nuclei would only be diluted by half, hence reducing surface area and precipitation rates by a factor of 2. However, as $\Omega_{Ar}$ is significantly reduced simultaneously, precipitation

405 rates are further reduced by a factor of 10 (see Figure A 4). Hence, overall precipitation would see a reduction by a factor of 20. This however, should slow down continuing precipitation initially, if on $CaCO_3$ particles, but not completely inhibit it (Zhong and Mucci, 1989). A possible explanation could be that dilution would have lowered $\Omega_{Ar}$ below the critical threshold for overcoming lattice mismatch, as most of the aragonite precipitation appears to be on the original seed mineral itself rather than on the newly formed aragonite (compare Figure 5c and 5d).

410 Overall, $CaCO_3$ precipitation can be avoided if the TA+500 µmol kg$^{-1}$ enriched sample is diluted 1:1, reaching an $\Omega_{Ar}$ of ~5.0. The quicker dilution takes place, the less $CaCO_3$ would precipitate prior. Similar results were found for a TA addition of +2000 µmol kg$^{-1}$, i.e., the ability to stop precipitation at an $\Omega_{Ar}$ of ~5.0, after a 1:7 dilution. However, only the 10 minutes and 1 hour dilutions seem to be suitable in an OAE context, as much more rapidly occurring aragonite precipitation at a higher initial $\Omega_{Ar}$ of about 16.7 would significantly reduce the $CO_2$ uptake efficiency. Furthermore, the difficulty to monitor precipitation form

415 simple TA measurements (as described above) would also mean that verification of permanent $CO_2$ removal is problematic. Hence, in order to assign carbon credits, TA additions have to be done in a way that rule out secondary $CaCO_3$ precipitation. This is the case for any type of TA addition, and is not specific to quick and hydrated lime.

Adding TA from land, as modelled by Feng et al. (2017), shows that the more TA is added, the higher coastal $\Omega_{Ar}$ would be. Staying clearly below the $\Omega_{Ar}$ 5 threshold, up to ~550 Gt of carbon in the form of $CO_2$ could be removed from the atmosphere

420 by 2100, corresponding to a reduction of about 260 ppm (Feng et al., 2017). The critical $\Omega_{Ar}$ threshold beyond which secondary $CaCO_3$ precipitation would be observed could be higher for other minerals, theoretically allowing for higher TA additions. However, it has to be kept in mind that in waters with high sediment load, often found in coastal settings, $CaCO_3$ could precipitate onto other mineral particles than those added to increase TA. This has been observed in river plumes (Wurgaft et al., 2021), on the Bahama Banks by resuspended sediments (Bustos-Serrano et al., 2009) and in the Red Sea following flash

425 flood deposition of resuspended sediments and particles (Wurgaft et al., 2016). Hence, even with minerals potentially allowing for higher TA additions, an $\Omega_{Ar}$ threshold of 5 might be safer to adopt. However, atmospheric $CO_2$ removal could be increased if TA would also be added to the open ocean, e.g., on ships of opportunity. Here, additions could be much higher as ship movement and rapid mixing within its wake would significantly dilute added TA (Caserini et al., 2021; Köhler et al., 2013) as opposed to coastal point source.

430 Finally, another option to increase atmospheric $CO_2$ uptake would be to not add mineral to seawater directly, but to first equilibrate it with air or $CO_2$ enriched flumes to atmospheric $pCO_2$ levels while dissolving. This would allow reaching an $\Omega_{Ar}$ of 5 when equilibrated with the atmosphere, as opposed to 3.3 when equilibration is slow and passive, after +250 µmol kg$^{-1}$ TA increase (Table 3). In this case, nearly 1000 instead of 250 µmol kg$^{-1}$ of TA could be added, allowing for almost 4 times the amount of atmospheric $CO_2$ to be removed (this number is highly sensitive to temperature, and ranges between ~3 and ~6
435    between 30 and 5 °C). However, this represent an extra step, which appears to be far more time and cost consuming than a simple mineral addition. It has also to be kept in mind that for the same $\Omega_{Ar}$ threshold, the amount of TA that can be added will increase with lower temperature, as of higher $CO_2$ solubility and hence naturally lower $\Omega_{Ar}$ in colder waters. At a salinity of 35 and at 5 °C, about three times as much TA can be dissolved as opposed to a temperature of 30 °C.

## 5 Conclusions

440    *Ocean alkalinity enhancement* is a promising negative emission technology. In order to maximise carbon dioxide ($CO_2$) uptake efficiency, secondary calcium carbonate ($CaCO_3$) precipitation has to be avoided. Here, we show that an increase of total alkalinity (TA) by 500 µmol kg$^{-1}$ led to aragonite precipitation, reducing the $CO_2$ uptake potential from about 0.8 moles per mole of alkalinity added to less than 0.2 moles. Precipitation was most likely onto CaO and Ca(OH)$_2$ mineral phases prior to full dissolution. In contrast, an addition of 250 µmol kg$^{-1}$ of TA did not result in $CaCO_3$ precipitation, suggesting that an

445    aragonite saturation state ($\Omega_{Ar}$) of about 5 is a safe upper limit. This is probably also the case for other minerals that would theoretically allow for higher TA additions as of potential precipitation onto naturally present mineral phases, such as resuspended sediments in coastal settings. Safely increasing the amount of TA that could be added to the ocean involves expanding to the open ocean by ships of opportunity, allowing major mixing and dilution of enriched seawater, equilibrating the seawater to atmospheric $CO_2$ levels during mineral dissolution, and targeting low rather than high temperature regimes.

## Data availability

450

Data will be made available on a publicly available repository upon final publication.

## Author contributions

CAM and KGS designed the initial experiments. All co-authors contributed to the initial data analysis and designing of follow-up experiments. CAM performed most of the sampling, and the data analyses with the help of KGS. CAM wrote the paper

455    with KGS, with inputs from their respective fields of expertise by all co-authors.

## Competing interests

The authors declare that they have no conflict of interest.

**Acknowledgements**

We would like to thank Marian Bailey for her help with ICPMS sample preparation, as well as Dr Nick Ward for his help with preliminary X-ray Diffraction analyses of the calcium powders. We are also thankful to Dr Matheus Carvalho de Carvalho for the particulate carbon analyses and Nadia Toppler for her help arranging the use of the SEM.

**Financial support**

This research is part of the PhD project of CAM that is funded by a Cat. 5 – SCU Grad School scholarship from the Southern Cross University, Lismore, Australia. The ICPMS analyses were made possible by the Australian Research Council grants number LE200100022 by RJB and KGS, and LE120100201 obtained by RJB.

# References

Bates, N., Best, M., Neely, K., Garley, R., Dickson, A., and Johnson, R.: Detecting anthropogenic carbon dioxide uptake and ocean acidification in the North Atlantic Ocean, Biogeosciences Discussions, 9, 2012.

Berner, R.: The role of magnesium in the crystal growth of calcite and aragonite from sea water, Geochimica et Cosmochimica Acta, 39, 489-504, 1975.

Boyd, P., Vivian, C., Boettcher, M., Chai, F., Cullen, J., Goeschl, T., Lampitt, R., Lenton, A., Oschlies, A., and Rau, G.: High level review of a wide range of proposed marine geoengineering techniques, 2019.

Bustos-Serrano, H., Morse, J. W., and Millero, F. J.: The formation of whitings on the Little Bahama Bank, Marine Chemistry, 113, 1-8, 2009.

Canadell, J. G., Le Quéré, C., Raupach, M. R., Field, C. B., Buitenhuis, E. T., Ciais, P., Conway, T. J., Gillett, N. P., Houghton, R., and Marland, G.: Contributions to accelerating atmospheric CO2 growth from economic activity, carbon intensity, and efficiency of natural sinks, Proceedings of the national academy of sciences, 104, 18866-18870, 2007.

Carter, B. R., Feely, R. A., Wanninkhof, R., Kouketsu, S., Sonnerup, R. E., Pardo, P. C., Sabine, C. L., Johnson, G. C., Sloyan, B. M., and Murata, A.: Pacific anthropogenic carbon between 1991 and 2017, Global Biogeochemical Cycles, 33, 597-617, 2019.

Caserini, S., Pagano, D., Campo, F., Abbà, A., De Marco, S., Righi, D., Renforth, P., and Grosso, M.: Potential of Maritime Transport for Ocean Liming and Atmospheric CO2 Removal, Frontiers in Climate, 3, 22, 2021.

Chang, R., Kim, S., Lee, S., Choi, S., Kim, M., and Park, Y.: Calcium carbonate precipitation for CO2 storage and utilization: a review of the carbonate crystallization and polymorphism, Frontiers in Energy Research, 5, 17, 2017.

Chen, T., Neville, A., and Yuan, M.: Calcium carbonate scale formation—assessing the initial stages of precipitation and deposition, Journal of Petroleum Science and Engineering, 46, 185-194, 2005.

Cyronak, T., Schulz, K. G., Santos, I. R., and Eyre, B. D.: Enhanced acidification of global coral reefs driven by regional biogeochemical feedbacks, Geophysical Research Letters, 41, 5538-5546, 2014.

Dickson, A. and Millero, F. J.: A comparison of the equilibrium constants for the dissociation of carbonic acid in seawater media, Deep Sea Research Part A. Oceanographic Research Papers, 34, 1733-1743, 1987.

Dickson, A. G.: Standards for ocean measurements, Oceanography, 23, 34-47, 2010.

Dickson, A. G., Sabine, C. L., and Christian, J. R.: Guide to best practices for ocean CO2 measurements, North Pacific Marine Science Organization2007.

Doney, S. C., Fabry, V. J., Feely, R. A., and Kleypas, J. A.: Ocean acidification: the other CO2 problem, Annual review of marine science, 1, 169-192, 2009.

Feng, E., Koeve, W., Keller, D. P., and Oschlies, A.: Model-Based Assessment of the CO2 Sequestration Potential of Coastal Ocean Alkalinization, Earth's Future, 5, 1252-1266, 2017.

Feng, E. Y., Keller, D. P., Koeve, W., and Oschlies, A.: Could artificial ocean alkalinization protect tropical coral ecosystems from ocean acidification?, Environmental Research Letters, 11, 074008, 2016.

Gafar, N. A. and Schulz, K. G.: A three-dimensional niche comparison of Emiliania huxleyi and Gephyrocapsa oceanica: reconciling observations with projections, Biogeosciences, 15, 3541-3560, 2018.

Gattuso, J.-P., Magnan, A., Billé, R., Cheung, W. W., Howes, E. L., Joos, F., Allemand, D., Bopp, L., Cooley, S. R., and Eakin, C. M.: Contrasting futures for ocean and society from different anthropogenic CO2 emissions scenarios, Science, 349, aac4722, 2015.

González, M. F. and Ilyina, T.: Impacts of artificial ocean alkalinization on the carbon cycle and climate in Earth system simulations, Geophysical Research Letters, 43, 6493-6502, 2016.

Goodwin, P., Brown, S., Haigh, I. D., Nicholls, R. J., and Matter, J. M.: Adjusting mitigation pathways to stabilize climate at 1.5 C and 2.0 C rise in global temperatures to year 2300, Earth's Future, 6, 601-615, 2018.

Harvey, L.: Mitigating the atmospheric CO2 increase and ocean acidification by adding limestone powder to upwelling regions, Journal of Geophysical Research: Oceans, 113, 2008.

Hoegh-Guldberg, O., Jacob, D., Taylor, M., Bolaños, T. G., Bindi, M., Brown, S., Camilloni, I., Diedhiou, A., Djalante, R., and Ebi, K.: The human imperative of stabilizing global climate change at 1.5° C, Science, 365, eaaw6974, 2019.

Hoegh-Guldberg, O., Mumby, P. J., Hooten, A. J., Steneck, R. S., Greenfield, P., Gomez, E., Harvell, C. D., Sale, P. F., Edwards, A. J., and Caldeira, K.: Coral reefs under rapid climate change and ocean acidification, science, 318, 1737-1742, 2007.

Ilyina, T., Wolf-Gladrow, D., Munhoven, G., and Heinze, C.: Assessing the potential of calcium-based artificial ocean alkalinization to mitigate rising atmospheric CO2 and ocean acidification, Geophysical Research Letters, 40, 5909-5914, 2013.

IPCC: Climate Change 2021: The Physical Science Basis. Contribution of Working Group I to the Sixth Assessment Report of the Intergovernmental Panel on Climate Change [Masson-Delmotte, V., P. Zhai, A. Pirani, S. L. Connors, C. Péan, S. Berger, N. Caud, Y. Chen, L. Goldfarb, M. I. Gomis, M. Huang, K. Leitzell, E. Lonnoy, J. B. R. Matthews, T. K. Maycock, T. Waterfield, O. Yelekçi, R. Yu and B. Zhou (eds.)]. Cambridge University Press. In Press., 2021.

520    Kheshgi, H. S.: Sequestering atmospheric carbon dioxide by increasing ocean alkalinity, Energy, 20, 915-922, 1995.

Köhler, P., Hartmann, J., and Wolf-Gladrow, D. A.: Geoengineering potential of artificially enhanced silicate weathering of olivine, Proceedings of the National Academy of Sciences, 107, 20228-20233, 2010.

Köhler, P., Abrams, J. F., Völker, C., Hauck, J., and Wolf-Gladrow, D. A.: Geoengineering impact of open ocean dissolution of olivine on atmospheric CO2, surface ocean pH and marine biology, Environmental Research Letters, 8, 014009, 2013.

525    Lenton, T. and Vaughan, N.: The radiative forcing potential of different climate geoengineering options. Atmos. Chem. Phys. Discuss., V, 2009.

Lewis, E. and Perkin, R.: The practical salinity scale 1978: conversion of existing data, Deep Sea Research Part A. Oceanographic Research Papers, 28, 307-328, 1981.

Lioliou, M. G., Paraskeva, C. A., Koutsoukos, P. G., and Payatakes, A. C.: Heterogeneous nucleation and growth of calcium carbonate on
530    calcite and quartz, Journal of colloid and interface science, 308, 421-428, 2007.

Lueker, T. J., Dickson, A. G., and Keeling, C. D.: Ocean pCO2 calculated from dissolved inorganic carbon, alkalinity, and equations for K1 and K2: validation based on laboratory measurements of CO2 in gas and seawater at equilibrium, Marine chemistry, 70, 105-119, 2000.

Marion, G., Millero, F. J., and Feistel, R.: Precipitation of solid phase calcium carbonates and their effect on application of seawater SA–T–P models, Ocean Science, 5, 285, 2009.

535    Mehrbach, C., Culberson, C., Hawley, J., and Pytkowicx, R.: Measurement of the apparent dissociation constants of carbonic acid in seawater at atmospheric pressure 1, Limnology and oceanography, 18, 897-907, 1973.

Millero, F., Huang, F., Zhu, X., Liu, X., and Zhang, J.-Z.: Adsorption and desorption of phosphate on calcite and aragonite in seawater, Aquatic Geochemistry, 7, 33-56, 2001.

Mongin, M., Baird, M. E., Lenton, A., Neill, C., and Akl, J.: Reversing ocean acidification along the Great Barrier Reef using alkalinity injection,
540    Environmental Research Letters, 16, 064068, 2021.

Montserrat, F., Renforth, P., Hartmann, J., Leermakers, M., Knops, P., and Meysman, F. J.: Olivine dissolution in seawater: implications for CO2 sequestration through enhanced weathering in coastal environments, Environmental science & technology, 51, 3960-3972, 2017.

Morse, J. W. and He, S.: Influences of T, S and PCO2 on the pseudo-homogeneous precipitation of CaCO3 from seawater: implications for whiting formation, Marine Chemistry, 41, 291-297, 1993.

545    Morse, J. W., Arvidson, R. S., and Lüttge, A.: Calcium carbonate formation and dissolution, Chemical reviews, 107, 342-381, 2007.

Morse, J. W., Gledhill, D. K., and Millero, F. J.: Caco3 precipitation kinetics in waters from the great Bahama bank:: Implications for the relationship between bank hydrochemistry and whitings, Geochimica et Cosmochimica Acta, 67, 2819-2826, 2003.

Ni, M. and Ratner, B. D.: Differentiating calcium carbonate polymorphs by surface analysis techniques—an XPS and TOF-SIMS study, Surface and Interface Analysis: An International Journal devoted to the development and application of techniques for the analysis of surfaces,
550    interfaces and thin films, 40, 1356-1361, 2008.

Pan, Y., Li, Y., Ma, Q., He, H., Wang, S., Sun, Z., Cai, W.-J., Dong, B., Di, Y., and Fu, W.: The role of Mg2+ in inhibiting CaCO3 precipitation from seawater, Marine Chemistry, 104036, 2021.

Renforth, P. and Henderson, G.: Assessing ocean alkalinity for carbon sequestration, Reviews of Geophysics, 55, 636-674, 2017.

Riebesell, U., Fabry, V. J., Hansson, L., and Gattuso, J.-P.: Guide to best practices for ocean acidification research and data reporting, Office
555    for Official Publications of the European Communities2011.

Riley, J. and Tongudai, M.: The major cation/chlorinity ratios in sea water, Chemical Geology, 2, 263-269, 1967.

Schulz, K. G., Bach, L. T., Bellerby, R. G., Bermúdez, R., Büdenbender, J., Boxhammer, T., Czerny, J., Engel, A., Ludwig, A., and Meyerhöfer, M.: Phytoplankton blooms at increasing levels of atmospheric carbon dioxide: experimental evidence for negative effects on prymnesiophytes and positive on small picoeukaryotes, Frontiers in Marine Science, 4, 64, 2017.

560    Tang, H., Wu, X., Xian, H., Zhu, J., Wei, J., Liu, H., and He, H.: Heterogeneous Nucleation and Growth of CaCO3 on Calcite (104) and Aragonite (110) Surfaces: Implications for the Formation of Abiogenic Carbonate Cements in the Ocean, Minerals, 10, 294, 2020.

The Royal Society and Royal Academy of Engineering: Greenhouse Gas Removal. See: https://royalsociety.org/-/media/policy/projects/greenhouse-gas-removal/royal-society-greenhouse-gas-removal-report-2018.pdf,

Uppstrom, L.: The boron/chlorinity ratio of deep-sea water from the Pacific Ocean, Deep Sea Res., 21, 161-162, 1974.

565    Wolf-Gladrow, D. A., Zeebe, R. E., Klaas, C., Körtzinger, A., and Dickson, A. G.: Total alkalinity: The explicit conservative expression and its application to biogeochemical processes, Marine Chemistry, 106, 287-300, 2007.

Wolf, S. E., Leiterer, J., Kappl, M., Emmerling, F., and Tremel, W.: Early homogenous amorphous precursor stages of calcium carbonate and subsequent crystal growth in levitated droplets, Journal of the American Chemical Society, 130, 12342-12347, 2008.

Wurgaft, E., Steiner, Z., Luz, B., and Lazar, B.: Evidence for inorganic precipitation of CaCO3 on suspended solids in the open water of the
570    Red Sea, Marine Chemistry, 186, 145-155, 2016.

Wurgaft, E., Wang, Z., Churchill, J., Dellapenna, T., Song, S., Du, J., Ringham, M., Rivlin, T., and Lazar, B.: Particle triggered reactions as an important mechanism of alkalinity and inorganic carbon removal in river plumes, Geophysical Research Letters, e2021GL093178, 2021.

Zeebe, R. E. and Wolf-Gladrow, D.: CO2 in seawater: equilibrium, kinetics, isotopes, 65, Gulf Professional Publishing2001.

575 Zhong, S. and Mucci, A.: Calcite and aragonite precipitation from seawater solutions of various salinities: Precipitation rates and overgrowth compositions, Chemical geology, 78, 283-299, 1989.

**Table 1: Summary of experimental conditions. Please note that for comparability, more TA was added in the liquid than the sieved approaches to match the theoretical increases in calcium carbonate saturation state (see Methods section for details).**

| TA Agent | TA target ($\mu$mol kg$^{-1}$) | Comments | Amount added in mg (or mL*) | Amount of natural seawater in kg | mg kg$^{-1}$ (or mL kg$^{-1}$*) | Theoretical TA addition ($\mu$mol kg-1) | Experiment duration | Additional samples apart from TA and DIC |
|---|---|---|---|---|---|---|---|---|
| **Sieved calcium minerals experiments** | | | | | | | | |
| CaO | 250 | Sieved in | 15.50 | 2015.90 | 7.69 | 274.21 | 47 days | N/A |
| CaO | 500 | Sieved in | 30.60 | 2004.50 | 15.27 | 544.42 | 47 days | TPC, POC and SEM samples |
| Ca(OH)$_2$ | 250 | Sieved in | 19.90 | 2001.90 | 9.94 | 268.34 | 28 days | N/A |
| Ca(OH)$_2$ | 500 | Sieved in | 37.40 | 2004.20 | 18.66 | 503.73 | 42 days | TPC, POC and SEM samples |
| **Na$_2$CO$_3$, particles and filtration experiments** | | | | | | | | |
| Na$_2$CO$_3$ | 1050 | 1M Na$_2$CO$_3$ solution | 1.05* | 2000.60 | 0.52 | 1050.32 | 42 days | N/A |
| Na$_2$CO$_3$ | 1050 | 1M Na$_2$CO$_3$ solution, plus quartz powder after 2 days | 1.05* | 2000.30 | 0.5 | 1050.16 | 48 days | TPC, POC and SEM samples |
| Ca(OH)$_2$ | 500 | Sieved in, filtered after 4 hours | 39.30 | 2004.30 | 19.61 | 529.30 | 48 days | N/A |
| **Dilution experiments** | | | | | | | | |
| Ca(OH)$_2$ | 500 | 1:1 dilution after 10min, 1 hour, 1 day and 1 week | 101.60 | 5132.50 | 19.80 | 534.36 | 14 days | TPC, POC and SEM samples |
| Ca(OH)$_2$ | 2000 | 1:7 dilution after 10min, 1 hour, 1 day and 1 week | 155.90 | 2003.80 | 77.80 | 2100.21 | 48 days | TPC, POC and SEM samples |

**Table 2: Comparison between the estimated PIC based on half the TA change between the theoretical maximum TA increase upon full dissolution of the alkaline material added and the measured TA at the end of the experiment (Table 1), the estimated PIC based on half the TA changes between the measured maximum TA increase and the measured TA at the end of the experiment, and the measured PIC from the particulate carbon analysis.**

| Experiment | PIC $\Delta TA_{Theo}$ ($\mu mol\ kg^{-1}$) | PIC $\Delta TA$ ($\mu mol\ kg^{-1}$) | Measured PIC ($\mu mol\ kg^{-1}$) |
|---|---|---|---|
| 500 TA – CaO Addition | 543.24 | 476.38 | 491.82 ±39.18 |
| 500 TA – Ca(OH)$_2$ Addition | 462.28 | 430.51 | 550.87 ±71.32 |
| 1050 TA – 1M Na$_2$CO$_3$ Addition + Quartz Particles | 627.20 | 639.07 | 397.37 ±24.03 |
| 500 TA – Ca(OH)$_2$ Addition | 107.05 | 66.20 | 89.51 ±4.27 |
| 2000 TA – Ca(OH)$_2$ Addition | 1718.83 | 1030.74 | 1331.48 ±50.73 |

**Table 3: Simulations of the changes in TA, DIC, $\Omega_{Ar}$, $pCO_2$ and $pH_T$ (total scale) after TA increases of 250, 500 and 1000 $\mu mol\ kg^{-1}$, assuming complete mineral dissolution without precipitation, a complete dissolution followed by as much $CaCO_3$ precipitated as the amount of TA added, and a complete dissolution followed by $CaCO_3$ precipitation until reaching an $\Omega_{Ar}$ of 2.0, before $CO_2$ re-equilibration to initial $pCO_2$. For each scenario, the amount of moles of $CO_2$ absorbed per moles of TA added has been calculated for comparison. The 500 $\mu mol\ kg^{-1}$ TA addition simulation is shown in Figure A 3, Appendix. *Note: the value for $\Omega_{Ar}$ is rounded to 1.00 but calculated at 0.997.**

| | Starting Conditions (salinity = 35, 19 °C) | TA +250 $\mu mol\ kg^{-1}$ No CaCO$_3$ precipitation | TA +500 $\mu mol\ kg^{-1}$ | | | | TA +1000 $\mu mol\ kg^{-1}$ | | | |
| --- | --- | --- | --- | --- | --- | --- | --- | --- | --- | --- |
| | | | No CaCO$_3$ Prec. | CaCO$_3$ Prec. = TA added | CaCO$_3$ Prec. until $\Omega_{Ar}$ of 2 | CO$_2$ uptake to pCO$_2$ ~416 $\mu atm$ | No CaCO$_3$ Prec. | CaCO$_3$ Prec. = TA added | CaCO$_3$ Prec. until $\Omega_{Ar}$ of 2 | CO$_2$ uptake to pCO$_2$ ~416 $\mu atm$ |
| TA ($\mu mol\ kg^{-1}$) | 2350 | 2600 | 2850 | 2350 | 1748 | 1748 | 3350 | 2350 | 1320 | 1320 |
| DIC ($\mu mol\ kg^{-1}$) | 2100 | 2100 | 2100 | 1850 | 1549 | 1588 | 2100 | 1600 | 1085 | 1216 |
| $\Omega_{Ar}$ | 2.80 | 5.53 | 8.45 | 5.34 | 2.00 | 1.66 | 14.57 | 7.89 | 2.00 | 1.00* |
| pCO$_2$ ($\mu atm$) | 416.2 | 175.1 | 91.5 | 135.6 | 319.2 | 416.4 | 29.6 | 48.2 | 144.81 | 416.7 |
| pH$_T$ | 8.04 | 8.38 | 8.61 | 8.42 | 8.02 | 7.93 | 8.97 | 8.73 | 8.20 | 7.82 |
| **After re-equilibration, i.e., pCO$_2$ ~416 $\mu atm$** | | | | | | | | | | |
| Final TA ($\mu mol\ kg^{-1}$) | 2350 | 2600 | 2850 | 2350 | 1748 | NA | 3350 | 2350 | 1320 | NA |
| Final DIC ($\mu mol\ kg^{-1}$) | 2100 | 2309 | 2517 | 2100 | 1588 | NA | 2926.5 | 2100 | 1216 | NA |
| Final $\Omega_{Ar}$ | 2.80 | 3.34 | 3.90 | 2.80 | 1.66 | NA | 5.14 | 2.80 | 1.00* | NA |
| Final pH$_T$ | 8.04 | 8.08 | 8.11 | 8.04 | 7.93 | NA | 8.17 | 8.04 | 7.82 | NA |
| CO$_2$ uptake (mole/mole TA) | NA | 0.84 | 0.83 | 0.50 | 0.08 | NA | 0.83 | 0.50 | 0.13 | NA |
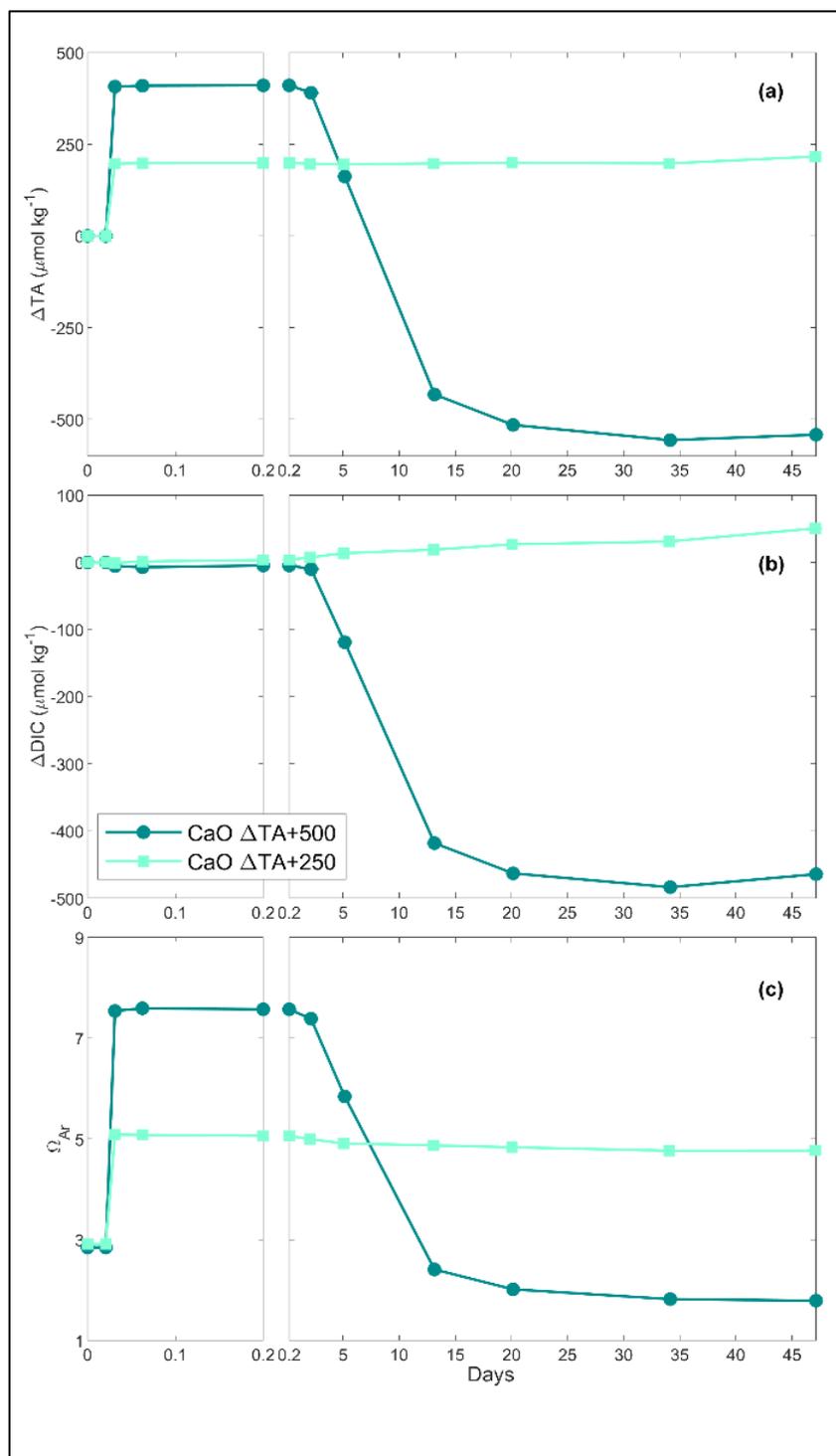
**Figure 1: Changes in TA (a), DIC (b) and $\Omega_{Ar}$ (c) over time following two CaO additions.**

590
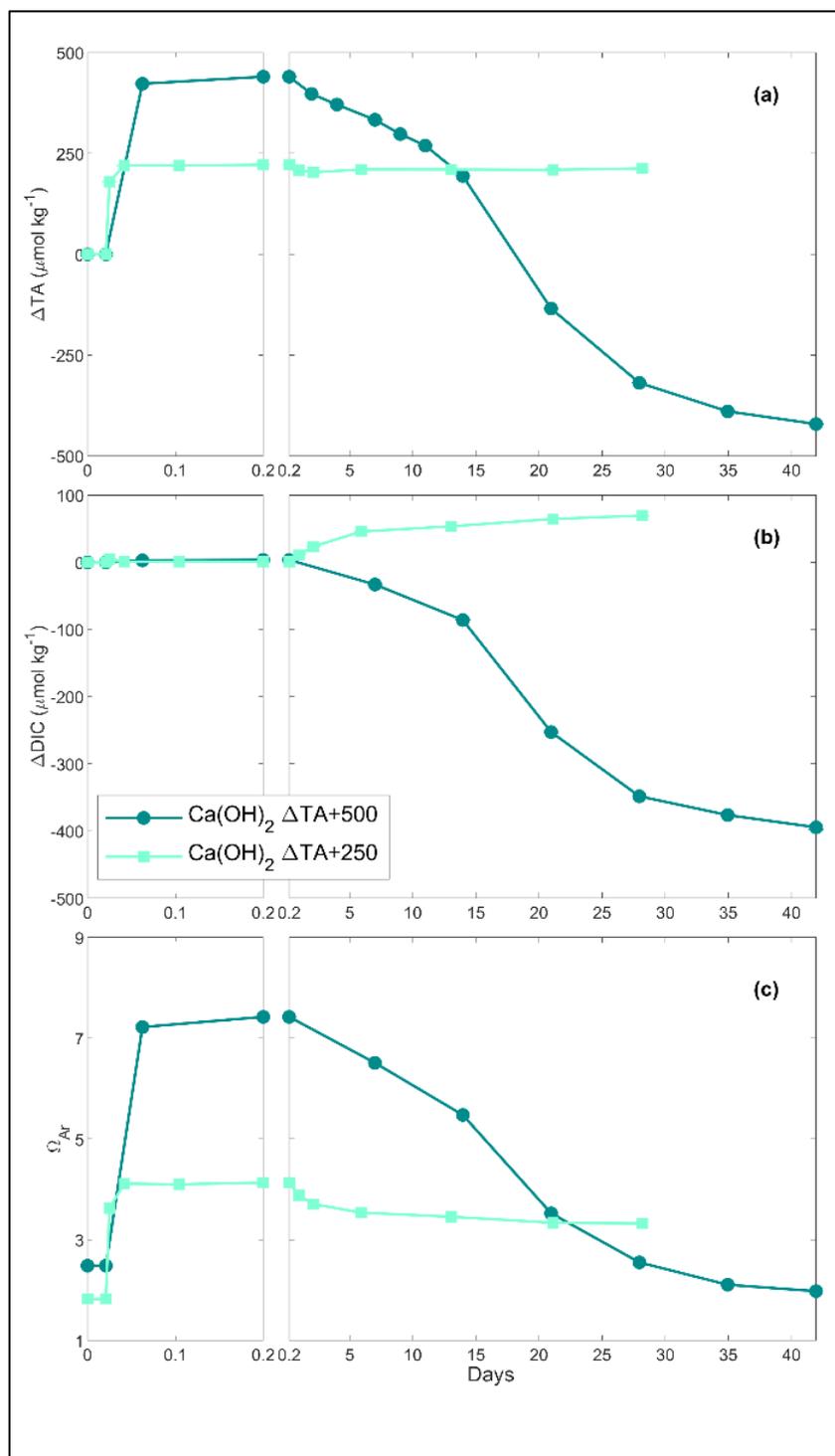
**Figure 2: Changes in TA (a), DIC (b) and $\Omega_{Ar}$ (c) of the samples over time following two Ca(OH)$_2$ additions.**
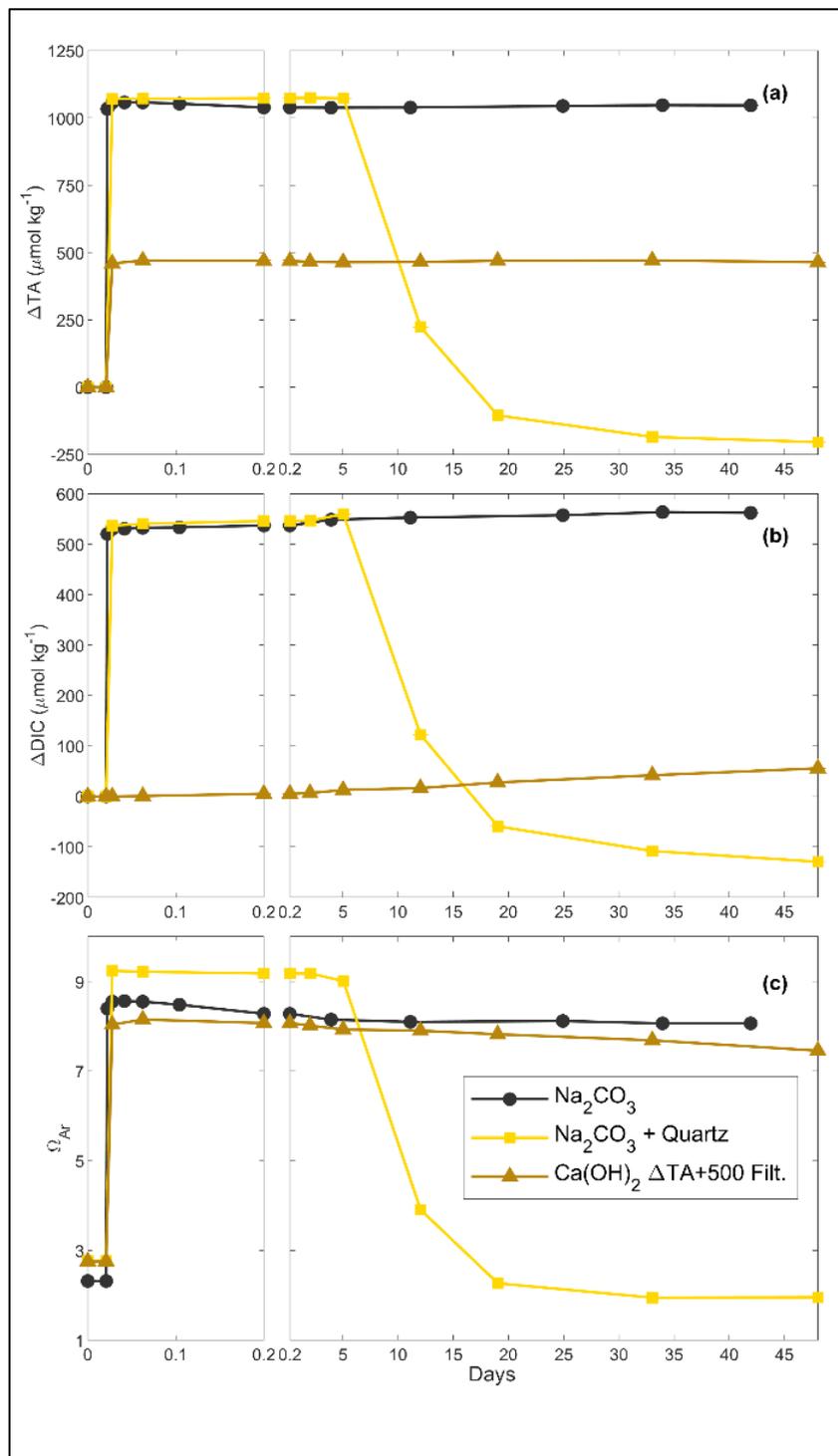
**Figure 3: Changes in TA (a), DIC (b) and $\Omega_{Ar}$ (c) over time following additions of Na₂CO₃, Na₂CO₃ plus quartz particles and Ca(OH)₂**
595  **followed by a filtration step (see Methods for details).**
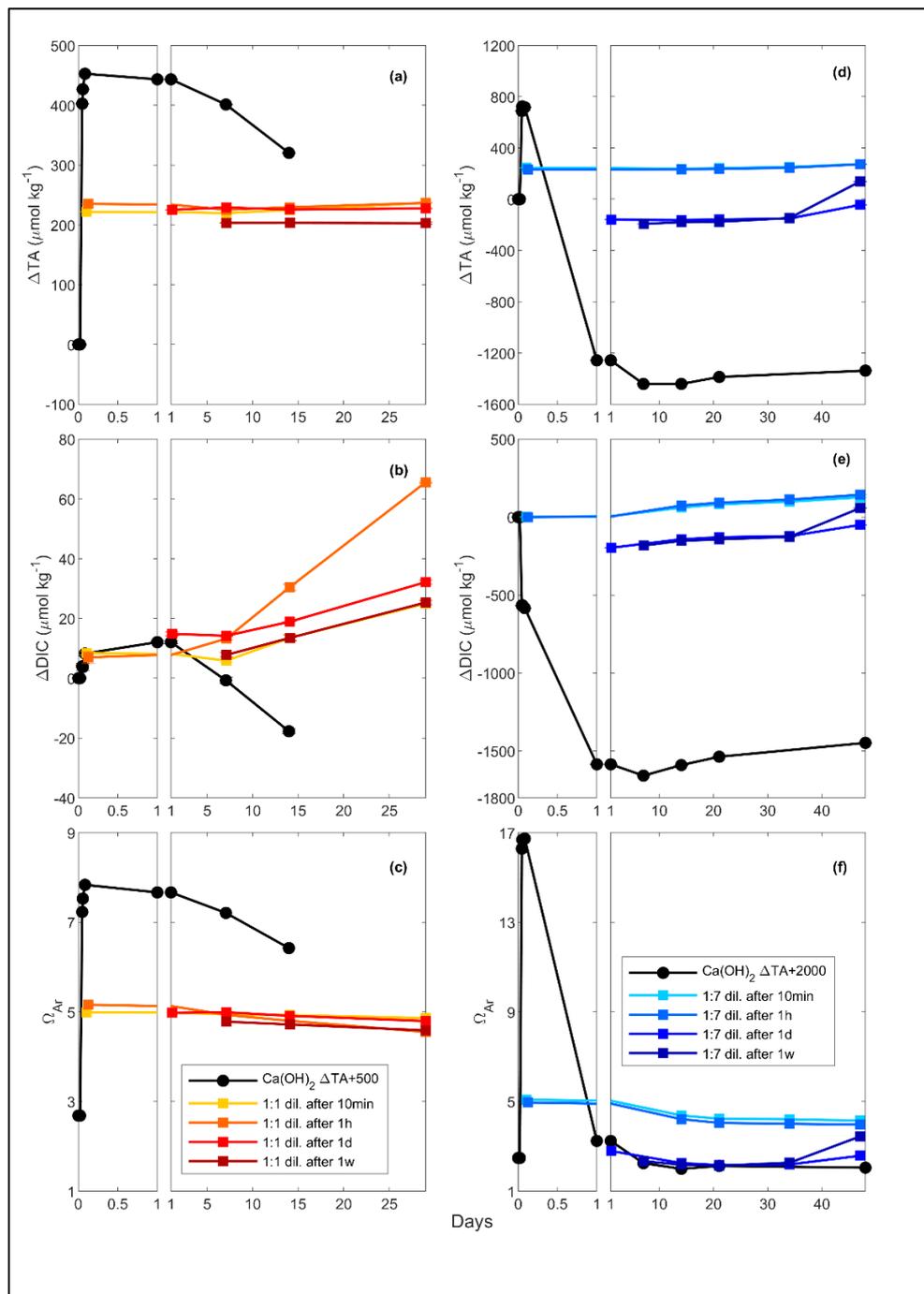
**Figure 4: Changes in TA (a and d), DIC (b and e) and $\Omega_{Ar}$ (c and f) following a TA addition of 500 and 2000 µmol kg$^{-1}$ respectively, by Ca(OH)$_2$ (black line), as well as following a 1:1 dilution or the 500 µmol kg$^{-1}$ TA addition (red and yellow lines) and a 1:7 dilution for the 2000 µmol kg$^{-1}$ TA addition (blue lines). The dilutions were performed after 10 minutes, 1 hour, 1 day and 1 week and earlier dilutions are represented by lighter colours.**

600
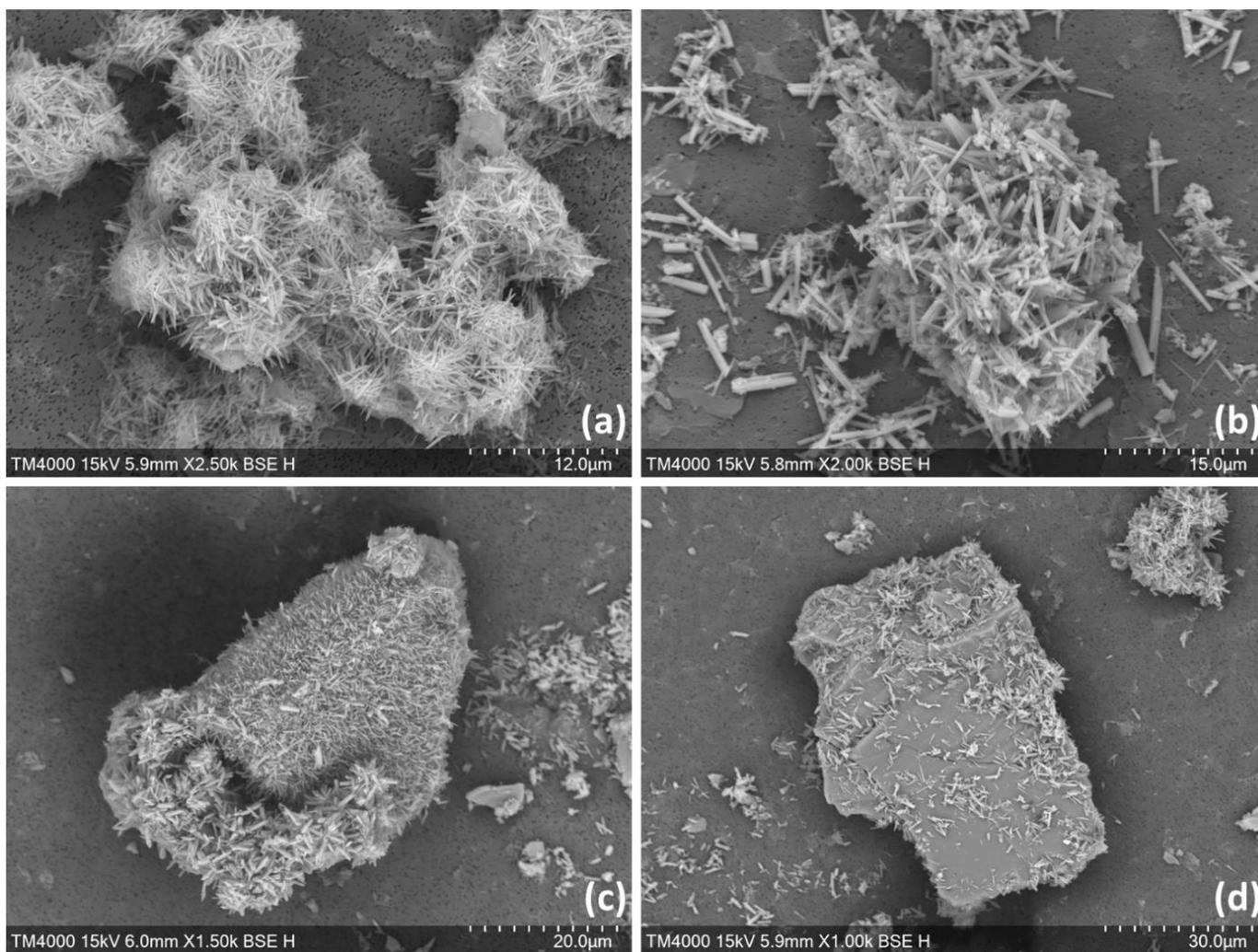
**Figure 5: SEM images from experiments with an increase in TA of ~500 μmol kg$^{-1}$ by CaO (a), Ca(OH)$_2$ (b) and with a TA increase of ~1050 μmol kg$^{-1}$ by 1M Na$_2$CO$_3$, followed by quartz particles addition ((c) and (d)).**

## Appendix

**Table A 1: Main chemical composition of the CaO and Ca(OH)$_2$ powders used for the TA increase experiments determined by ICPMS analysis.**

| CaO Powder | | | Ca(OH)$_2$ Powder | | |
|---|---|---|---|---|---|
| **Element** | **mg g$^{-1}$** | **St. Dev.** | **Element** | **mg g$^{-1}$** | **St. Dev.** |
| Calcium | 545.15 | 70.92 | Calcium | 529.79 | 117.30 |
| Magnesium | 2.10 | 0.23 | Magnesium | 6.87 | 1.98 |
| Silicon | 2.02 | 1.79 | Silicon | 2.70 | 1.12 |
| Aluminium | 0.50 | 0.19 | Aluminium | 1.98 | 0.77 |
| Iron | 0.32 | 0.10 | Iron | 0.91 | 0.34 |
| Manganese | 0.11 | 0.01 | Potassium | 0.43 | 0.23 |
| Potassium | 0.03 | 0.00 | Titanium | 0.07 | 0.03 |
| Phosphorus | 0.02 | 0.02 | Manganese | 0.05 | 0.01 |
| Titanium | 0.02 | 0.01 | Phosphorus | 0.04 | 0.01 |
| Chromium | 0.01 | 0.01 | Bromine | 0.03 | 0.01 |
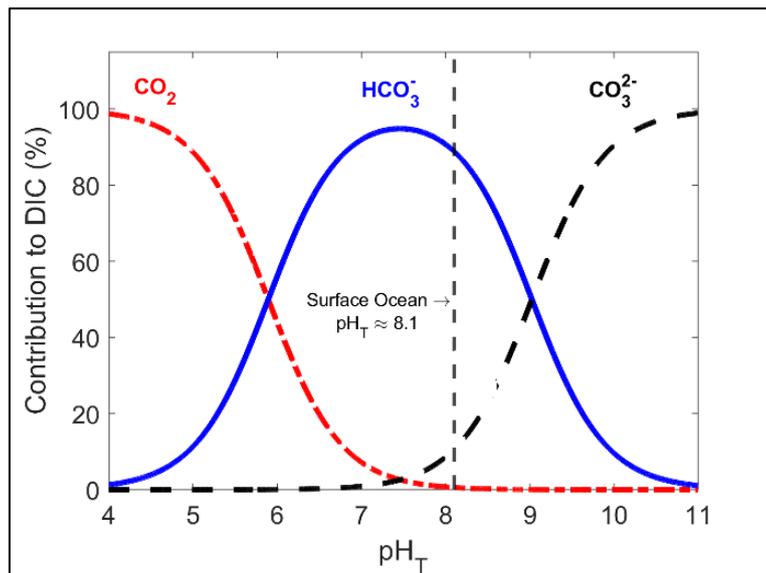
**Figure A 1: Relative contribution of dissolved CO$_2$, HCO$_3^-$ and CO$_3^{2-}$ to total dissolved inorganic carbon in seawater as a function of pH$_T$ (total scale), also known as Bjerrum plot (based on the carbonic acid equilibrium constant from Mehrbach et al. (1973) and refitted by Dickson and Millero (1987)), at 25 °C and salinity of 35, with the current surface ocean pH average represented by the dashed line (pH$_T$ ~8.1).**
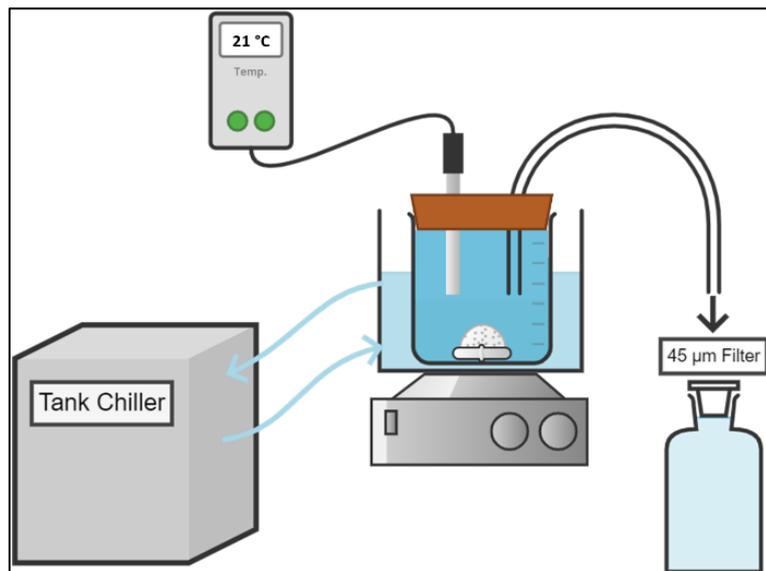
620    **Figure A 2: Conceptual diagram of the experimental setup used for the dissolution of alkaline mineral**s
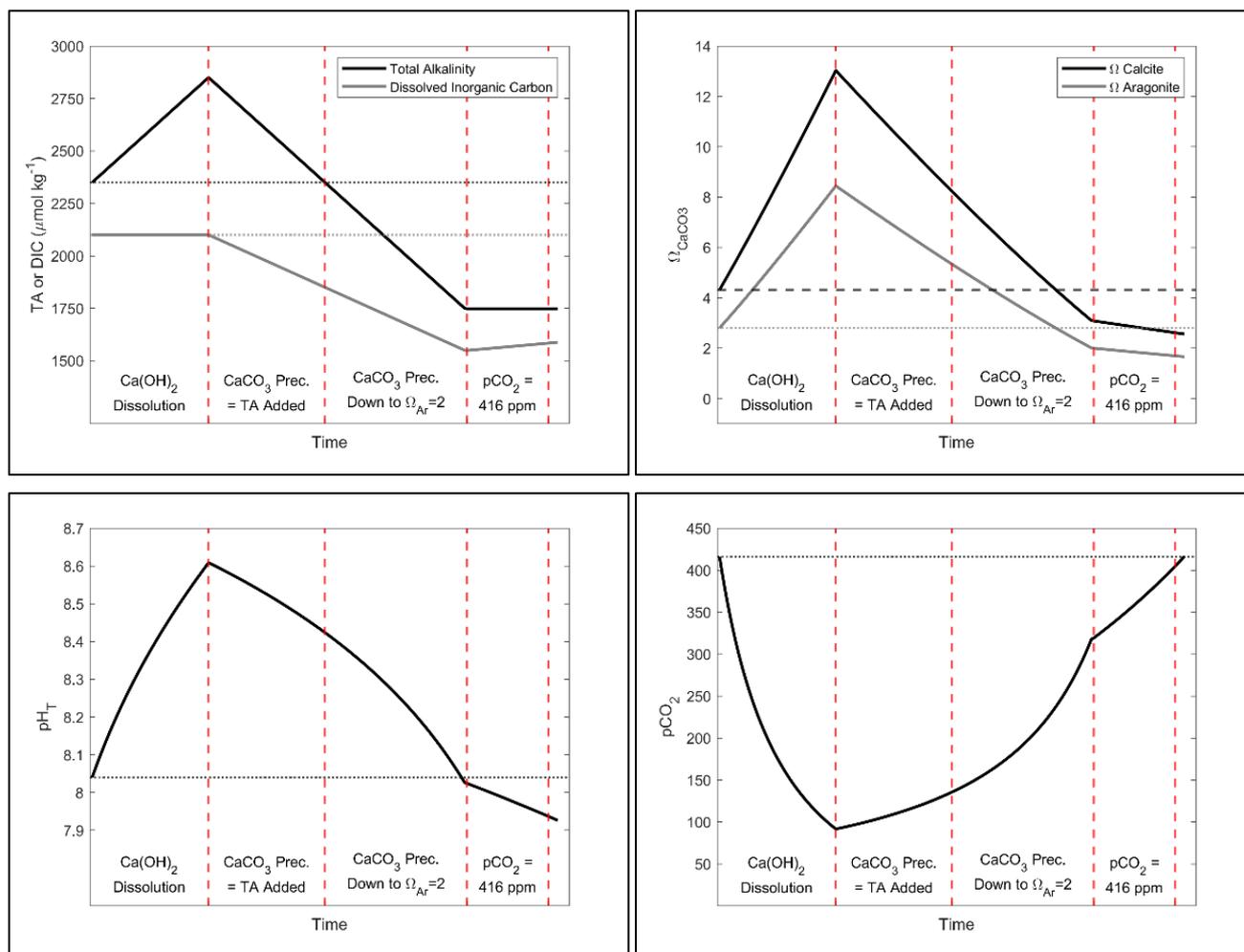
625

**Figure A 3: Simulation of the changes in TA, DIC, $\Omega_{Ca}$, $\Omega_{Ar}$, pCO₂ and pH$_T$ after addition of 500 µmol kg$^{-1}$ of alkalinity. Four important steps are presented: first assuming the complete Ca(OH)₂ dissolution without CaCO₃ precipitation, second assuming as much CaCO₃ precipitation as the amount of TA added, third assuming CaCO₃ precipitation happening until reaching $\Omega_{Ar}$ = 2.0 and fourth CO₂ uptake until equilibrium is reached between atmospheric and seawater pCO₂ of ~416 ppm.**

630
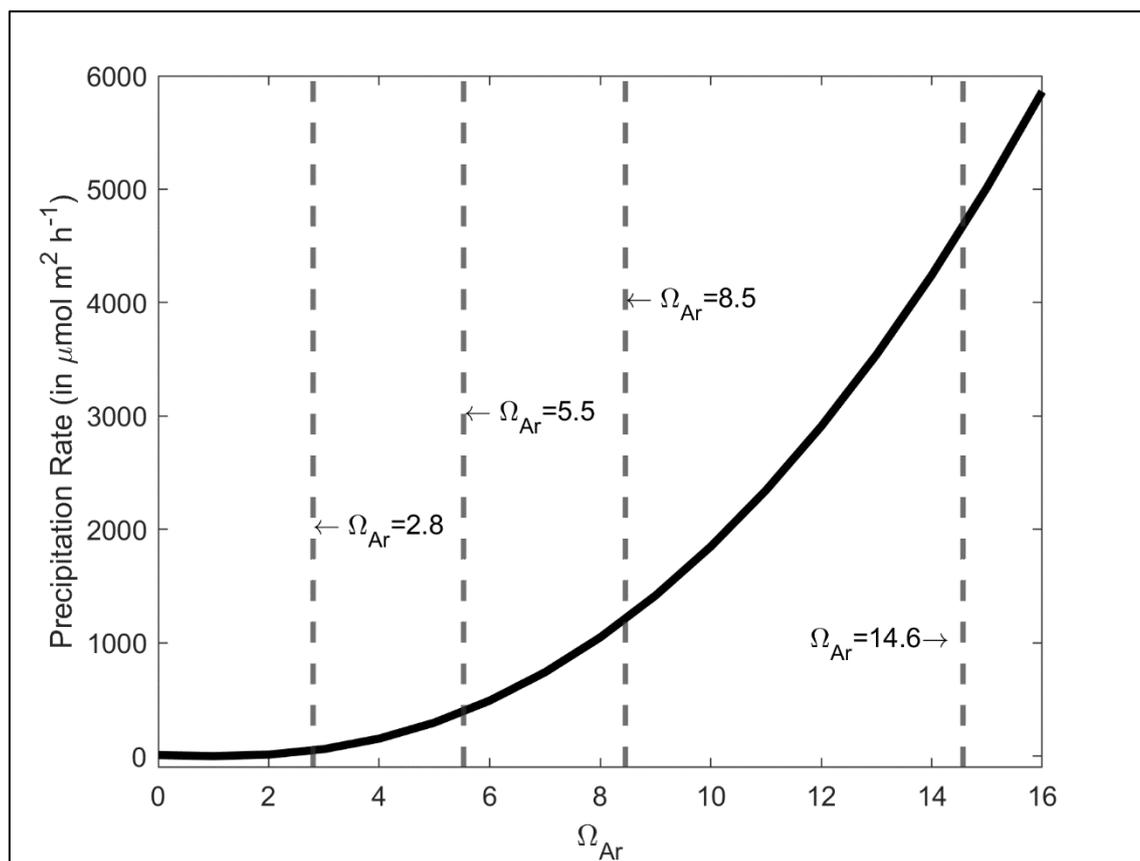
**Figure A 4: Aragonite precipitation rate onto CaCO₃ seed crystals in µmol m⁻² h⁻¹ as a function of $\Omega_{Ar}$, based on the calculation of Zhong and Mucci (1989) at 25 °C and for a salinity of 35. The values of $\Omega_{Ar}$ for the starting conditions, following a +250, +500 and +1000 µmol kg-1 TA increase are presented by the grey dashed lines, i.e., 2.8, 5.5, 8.5 and 14.6 respectively.**